Research Article **Open Access**

Ioannis G. Raftoyiannis* and George T. Michaltsos

The Influence of the Load Model and other Parameters on the Dynamic Behavior of Curved-in-Plane Bridges

DOI 10.1515/cls-2016-0019
Received Apr 13, 2016; accepted Jun 15, 2016

Abstract: This paper deals with the dynamic behavior of curved-in-plane bridges where the effect of the bridge curvature radius, the moving load (vehicle) speed, the truck cant angle, the deck surface conditions and, mainly, the response accuracy depending on the vehicle model used are investigated. Besides the above parameters, the influence of several loading models is studied as well, especially the models of a concentrated load, a damped mass-load, a sequence of two concentrated loads and a real vehicle as well as a damped vehicle, where its width is taken into account. A 3-DOF model is considered for the analysis of the bridge, while the theoretical formulation is based on a continuum approach, which has been widely used in the literature to analyze such bridges.

Keywords: Bridge dynamics; curved bridges; moving loads; damped vehicle

1 Introduction

Numerous studies have been reported during the last 100 years dealing with the dynamic response of railway bridges and later of highway bridges, under the influence of moving loads. Extensive references on the literature for this subject can be found in the excellent book of Frýba [1].

Two early contributions in this area presented by Stokes [2] and Zimmerman [3] are very interesting. In 1905, Krýlov [4] presented a complete solution to the problem of the dynamic behavior of a prismatic bar under a load of constant magnitude moving with constant velocity. In 1922, Timoshenko [5] solved the same problem but for a harmonic pulsating moving force. Another pioneer work on this subject was presented in 1934 by Inglis [6], in which numerous parameters were taken into account. In 1951, Hillerborg [7] presented an analytical solution to the previous problem by means of the Fourier method.

Despite the availability of powerful computers, most of the methods used today for analyzing bridge vibration problems are essentially based on the Inglis's or Hillerborg's early techniques. Relevant publications are ones by Stending [8], Honda *et al.* [9], Gillespi [10], Green and Cebon [11], Lee [12], Michaltsos *et al.* [13], Xu and Genin [14], Foda and Abduljabbar [15] and Michaltsos [16, 17].

In engineering practice and despite the large number of studies for over 50 years, bridges (as well as other structures) have been designed to account for dynamic loads by just increasing the design live loads by a semi-empirical "impact factor" or "dynamic load allowance".

Recently, many research programs dealing with the effect of the characteristics of a bridge or a vehicle on the dynamic response of a bridge have been developed such as: the programs in U.S.A [18], in U.K. and Canada [19], in the Organization for Economic Cooperation and Development (O.E.C.D.) [20], in Switzerland [21] etc. Among the important studies in this field, one must especially refer to the important experimental research by Cantieri [22] dealing with different models of moving loads.

Curved-in-plane bridges made from reinforced concrete or steel material are very common as elements of highway access, ramps and viaduct interchanges, while they are often the only solution in special territory conditions. A wide field of research is the one of seismic behavior of curved-in-plane bridges.

The majority of experimental and numerical research on curved-in-plane bridges was done in the USA in the late 1960s and early 1970s by Mozer and Culver [23], Culver [24] and Brennan [25]. This research continued in the 1990s by Yoo and Carbine [26]; Zureick *et al.* [27] and was used to improve the American Association of State Highway and Transportation Officials (AASHTO) specifications

***Corresponding Author: Ioannis G. Raftoyiannis:** Department of Civil Engineering, National Technical University of Athens, Greece 15780; Email: rafto@central.ntua.gr; Tel.: +30-210-7722454; Fax +30-210-7722482
George T. Michaltsos: Department of Civil Engineering, National Technical University of Athens, Greece 15780; Tel.: +30-210-7723443

regarding this topic. The aforementioned research mainly addressed steel bridges.

The seismic behavior of bridges is principally influenced by the seismic response of the substructures, such as bridge columns, abutments and foundations. In fact, design codes such as the Eurocodes in Europe (CEN) [28] and the Caltrans Seismic Design Criteria in California (Caltrans [29]) assume that the bridge deck remains elastic during a seismic event, and that the energy introduced by the ground motion is dissipated by either the substructures or specific seismic isolation and/or damping devices.

Parametric analyses related to the seismic behavior of curved bridges have been carried out recently by Abdel-Salam and Heins [30], Wu and Najjar [31] and Linzell and Nadakuditi [32] who highlighted that the radius of curvature had the most significant influence on the seismic response of curved-in-plane steel I-girder simply supported bridges. One must also mention the work of Dimitrakopoulos and Zeng [33], who studied the interaction of trains in curved-in-plane railway bridges and also the paper of Tondini and Stojadinovic [34] who studied the seismic behavior of curved-in-plane bridges.

After the two previous publications by Avraam and Michlatsos [35] and Raftoyiannis and Michaltsos [36], the present work deals with the dynamic behavior of curved-in-plane bridges where the effect of the radius of curvature, the vehicle speed, the truck cant angle, the deck surface conditions and, mainly, the response accuracy depending on the vehicle model used are thoroughly examined.

Besides the above parameters, the influence of several loading models is studied as well, especially the models of a concentrated load, a damped mass-load, a sequence of two concentrated loads and a real vehicle as well as a damped vehicle, where its width is taken into account. A 3-DOF model is considered for the analysis of the bridge, while the theoretical formulation is based on a continuum approach, which has been widely used in the literature to analyze such bridges.

2 Mathematical formulation

2.1 The equations of motion

Let us consider the deck of a bridge that is shown in Fig. 1 by the gravity-center line of its cross-sections (OS).

The bridge is curved-in-plane with radius of curvature R and thus, its length L is given by the relation $L = R \cdot \alpha$, where α is the sectorial angle corresponding to length L.

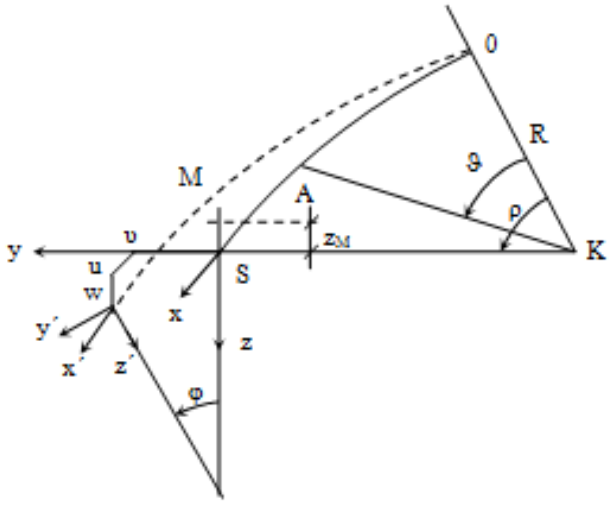

Figure 1: Geometrical notations and displacements for a curved bridge deck.

An arbitrary point A can be determined by the angle ϑ. Assuming that the distance z_M between the shear center M and the gravity center S is very small compared to the radius R, one can consider the torsional moment m_x acting about the gravity center axis (instead of the shear center axis).

According to the theory of curved beams with thin-walled cross-sections, the following equations are valid [36]:

$$
\begin{aligned}
& EJ_z v'''' + \frac{2EJ_z}{R^2} \cdot v'' + \frac{EJ_z}{R^4} \cdot v + c_y \dot{v} + m\ddot{v} = q_y \\
& \left(EJ_y - \frac{EJ_\omega}{R^2}\right) w'''' + \frac{GJ_d}{R^2} \cdot w'' - \frac{EJ_y - GJ_d}{R} \cdot \phi'' - \frac{EJ_\omega}{R} \\
& \qquad \cdot \phi'''' + c_z \dot{w} + m\,\ddot{w} = q_z \\
& EJ_\omega \phi'''' - GJ_d\,\phi'' - \frac{EJ_y}{R^2} \cdot \phi + \frac{EJ_\omega}{R} \\
& \qquad \cdot w'''' + \frac{EJ_y - GJ_d}{R} \cdot w'' + c_\phi \dot{\phi} \\
& \qquad + J_{px}\ddot{\phi} = m_x
\end{aligned}
\tag{1}
$$

where q_y, q_z and m_x are the internal forces developed in the cross-section at $x = R{\cdot}\alpha$, while J_{px} is the torsional mass-moment of inertia about the x-axis. In the present analysis, we will proceed for the usual case where $m_y = m_z = 0$ (for the directions and axes x, y, z, see Fig. 1).

For the following analysis and in order to apply the Galerkin method, a suitable set of expressions for the displacements v, w, and φ is required.

3 Set of expressions v, w, φ

Considering the case of a free vibrating beam and neglecting, for instant, the effect of the torsion on the vertical bending, eqs (1) become:

$$EJ_z v'''' + \frac{2EJ_z}{R^2}\cdot v'' + \frac{EJ_z}{R^4}\cdot v + c_y\dot{v} + m\ddot{v} = 0 \tag{2a}$$

$$\left(EJ_y - \frac{EJ_\omega}{R^2}\right) w'''' + \frac{GJ_d}{R^2}\cdot w'' + c_z\dot{w} + m\ddot{w} = 0 \tag{2b}$$

$$EJ_\omega\phi'''' - GJ_d\phi'' - \frac{EJ_y}{R^2}\cdot\phi + \frac{EJ_\omega}{R} \cdot w'''' + \frac{EJ_y - GJ_d}{R}\cdot w'' + c_\phi\dot{\phi} + J_{px}\ddot{\phi} = 0 \tag{2c}$$

Equation (2a) shows that the lateral motion is independent of the other two, while the vertical and torsional ones are coupled. Hence, one can set:

$$v(x,t) = Y(x)\cdot T_y(t) \tag{2d}$$

$$w(x,t) = Z(x)\cdot T_z(t) \tag{2e}$$

$$\phi(x,t) = \Phi(x)\cdot T_z(t) \tag{2f}$$

3.1 The lateral motion

Introducing eq. (2d) into eq. (2a), one obtains the following uncoupled equations:

$$EI_z Y''''(x) + \frac{2EI_z}{R^2}Y''(x) + \frac{EI_z}{R^4}Y(x) - m\omega_y^2 Y(x) = 0 \tag{3a}$$

$$\ddot{T}_y + \frac{c_y}{m}\dot{T}_y + \omega_y^2 T_y = 0 \tag{3b}$$

Solution of eq. (3a) gives the eigenshapes of the lateral motion:

$$Y_n(x) = c_1\left(\sin\lambda_{1n}x + \frac{\sin\lambda_{1n}L}{\operatorname{Sinh}\lambda_{2n}L}\cdot\operatorname{Sinh}\lambda_{2n}x\right) \tag{3c}$$

$$\text{where :}\quad \lambda_{1n} = \sqrt{\frac{1}{R^2} + \sqrt{\frac{m\omega_{yn}^2}{EJ_z}}}, \tag{3d}$$

$$\lambda_{2n} = \sqrt{-\frac{1}{R^2} + \sqrt{\frac{m\omega_{yn}^2}{EJ_z}}} \tag{3e}$$

$$\text{and :}\quad \omega_{yn}^2 = \frac{EJ_z}{m}\cdot\left(\frac{n^2\pi^2}{L^2} - \frac{1}{R^2}\right)^2 \tag{3f}$$

3.1.1 The vertical-torsional motion

Introducing eqs (2e, 2f) into eqs (2b, 2c), one obtains the following equations:

$$\left(EJ_y - \frac{EJ_\omega}{R^2}\right) Z'''' + \frac{GJ_d}{R^2}\cdot Z'' - m\omega_z^2 Z = 0 \tag{4a}$$

$$EJ_\omega\Phi'''' - GJ_d\Phi'' - \frac{EJ_y}{R^2}\cdot\Phi + \frac{EJ_\omega}{R}\cdot Z'''' + \frac{EJ_y - GJ_d}{R}\cdot Z'' - J_{px}\omega_z^2\Phi = 0 \tag{4b}$$

$$\ddot{T}_z + \frac{c_z}{m}\dot{T} + \omega_z^2 T_z = 0 \tag{4c}$$

Equation (4a) gives:

$$Z_n(x) = c_1\left(\sin k_{1n}x + \frac{\sin k_{1n}L}{\operatorname{Sinh} k_{2n}L}\cdot\operatorname{Sinh} k_{2n}x\right) \tag{4d}$$

where:

$$k_{1n} = \sqrt{\frac{GJ_d}{2(R^2EJ_y - EJ_\omega)} + \sqrt{\left(\frac{GJ_d}{2(R^2EJ_y - EJ_\omega)}\right)^2 + \frac{R^2m\omega_{zn}^2}{R^2EJ_y - EJ_\omega}}} \tag{4e}$$

$$k_{2n} = \sqrt{-\frac{GJ_d}{2(R^2EJ_y - EJ_\omega)} + \sqrt{\left(\frac{GJ_d}{2(R^2EJ_y - EJ_\omega)}\right)^2 + \frac{R^2m\omega_{zn}^2}{R^2EJ_y - EJ_\omega}}} \tag{4f}$$

and

$$\omega_{zn}^2 = \frac{R^2EJ_y - EJ_\omega}{R^2m}\cdot\frac{n^2\pi^2}{L^2}\cdot\left(\frac{n^2\pi^2}{L^2} + \frac{GJ_d}{R^2EJ_y - EJ_\omega}\right) \tag{4g}$$

The second of eqs (4) becomes:

$$EJ_\omega\Phi_n'''' - GJ_d\Phi_n'' - \frac{EJ_y}{R^2}\Phi_n - \omega_{zn}^2 J_{px}\Phi_n = -\frac{EJ_y}{R}Z_n'''' - \frac{EJ_y - GJ_d}{R}Z_n''$$

The above due to the first of eqs (4) becomes:

$$EJ_\omega\Phi''''_n - GJ_d\Phi''_n - \frac{EJ_y}{R^2}\Phi_n - \omega_{zn}^2 J_{px}\Phi_n = \zeta_{1n}\sin k_{1n}x + \zeta_{2n}\sinh k_{2n}x \tag{5a}$$

$$\text{where :}\quad \zeta_{1n} = k_{1n}^2\left(-k_{1n}^2\frac{EJ_\omega}{R} + \frac{EJ_y - GJ_d}{R}\right) \tag{5b}$$

$$\zeta_{2n} = -k_{2n}^2\left(k_{2n}^2\frac{EJ_\omega}{R} + \frac{EJ_y - GJ_d}{R}\right)\frac{\sin k_{1n}L}{\sinh k_{2n}L} \tag{5c}$$

The solution of the above equation is:

$$\Phi_n(x) = c_1\sin\mu_{1n}x + c_2\cos\mu_{1n}x + c_3\sinh\mu_{2n}x$$

$$+ \cosh \mu_{2n} x + A_n \sin k_{1n} x + B_n \cos k_{2n} x \tag{5d}$$

where:

$$A_n = \frac{\zeta_{1n}}{EJ_\omega k_{1n}^4 + GJ_d k_{1n}^2 - EJ_\omega / R^2 - \omega_{zn}^2 J_{px}} \tag{5e}$$

$$B_n = \frac{\zeta_{2n}}{EJ_\omega k_{1n}^4 - GJ_d k_{1n}^2 - EJ_\omega / R^2 - \omega_{zn}^2 J_{px}} \tag{5f}$$

$$\mu_{1n} = \sqrt{-\frac{GJ_d}{2EJ_\omega} + \sqrt{\left(\frac{GJ_d}{2EJ_\omega}\right)^2 + \frac{J_{px}\,\omega_{\phi n}^2}{EJ_\omega} + \frac{J_y}{R^2 J_\omega}}} \tag{5g}$$

$$\mu_{2n} = \sqrt{\frac{GJ_d}{2EJ_\omega} + \sqrt{\left(\frac{GJ_d}{2EJ_\omega}\right)^2 + \frac{J_{px}\,\omega_{\phi n}^2}{EJ_\omega} + \frac{J_y}{R^2 J_\omega}}} \tag{5h}$$

The boundary conditions are: $\Phi(0) = \Phi(L) = \Phi''(0) = \Phi''(L) = 0$, from which one can determine:

$$c_{2n} = 0 \tag{6a}$$

$$c_{4n} = 0 \tag{6b}$$

$$c_{1n} = \frac{-A_n(k_{1n}^2 + \mu_{1n}^2)\sin k_{1n}L + B_n(k_{2n}^2 - \mu_{2n}^2)\sinh k_{2n}L}{(\mu_{1n}^2 + \mu_{2n}^2)\sin \mu_{1n}L} \tag{6c}$$

$$c_{3n} = \frac{A_n(k_{1n}^2 - \mu_{1n}^2)\sin k_{1n}L - B_n(k_{2n}^2 + \mu_{2n}^2)\sinh k_{2n}L}{(\mu_{1n}^2 + \mu_{2n}^2)\sinh \mu_{2n}L} \tag{6d}$$

and finally:

$$\Phi_n(x) = c_{1n}\sin \mu_{1n} x + c_{3n}\sinh \mu_{2n} x + A_n \sin k_{1n} x + B_n \cos k_{2n} x \tag{6e}$$

4 The free vibrating bridge

The equations for the free motion of the bridge are:

$$EJ_z v'''' + \frac{2EJ_z}{R^2}\cdot v'' + \frac{EJ_z}{R^4}\cdot v + m\ddot{v} = 0 \tag{7a}$$

$$\left(EJ_y - \frac{EJ_\omega}{R^2}\right) w'''' + \frac{GJ_d}{R^2}\cdot w'' - \frac{EJ_y - GJ_d}{R}\cdot \phi'' - \frac{EJ_\omega}{R}\cdot \phi'''' + m\ddot{w} = 0 \tag{7b}$$

$$EJ_\omega \phi'''' - GJ_d \phi'' - \frac{EJ_y}{R^2}\cdot \phi + \frac{EJ_\omega}{R}\cdot w'''' + \frac{EJ_y - GJ_d}{R}\cdot w'' + J_{px}\ddot{\phi} = 0 \tag{7c}$$

4.1 The horizontal motion

The first of eqs (7) is independent of the other two. Therefore, the eigenfrequencies and shape functions are given by eqs (3c, 3d, 3e, 3f).

4.2 The coupled vertical-torsional motion

In order to solve eqs (7b, 7c), one can search for a solution of the form:

$$w(x,t) = W(x)\cdot T(t) \tag{8a}$$

$$\phi(x,t) = \Theta(x)\cdot T(t) \tag{8b}$$

Introducing eqs (8) into eqs (7b, 7c), the following differential system is obtained:

$$S_1 \cdot W'''' + \frac{GJ_d}{R^2}\cdot W'' - S_2 \cdot \Theta'' - \frac{EJ_\omega}{R}\cdot \Theta'''' - m\omega^2 W = 0 \tag{9a}$$

$$EJ_\omega \Theta'''' - GJ_d\,\Theta'' - \frac{EJ_y}{R^2}\cdot \Theta + \frac{EJ_\omega}{R}\cdot W'''' + S_2 \cdot W'' - J_{px}\omega^2 \Theta = 0 \tag{9b}$$

$$\text{where :}\quad S_1 = EJ_z - \frac{EJ_\omega}{R^2}, \quad S_2 = \frac{EJ_z - GJ_d}{R} \tag{9c}$$

In order to apply the Galerkin procedure, one can set:

$$W_\rho(x) = a_{\rho 1} Z_1(x) + a_{\rho 2} Z_2(x) + \cdots + a_{\rho n} Z_n(x) \tag{10a}$$

$$\Theta_\rho(x) = b_{\rho 1} \Phi_1(x) + b_{\rho 2} \Phi_2(x) + \cdots + b_{\rho n} \Phi_n(x) \tag{10b}$$

where a_i and b_i are unknown coefficients to be determined and Z_i, Φ_i, are arbitrarily chosen functions of x, which satisfy the boundary conditions. As such functions, the expressions given by eqs (4a) and (6e) are chosen. The functions W_k and Θ_k, corresponding to the eigenfrequency ω_k are determined as follows.

Introducing eqs (10) into eqs (9), multiplying the outcome successively the first by $Z_1, Z_2, \ldots, Z_n$ and the second by $\Phi_1, \Phi_2, \ldots, \Phi_n$, and integrating from 0 to L, one obtains the following linear homogeneous system of equations with unknowns the coefficients a_{ki} and b_{ki}.

$$\sum_{i=1}^{n} a_{\rho i}\left(S_1 \int_0^L Z_i'''' Z_\sigma dx + \frac{GJ_d}{R^2}\int_0^L Z_i'' Z_\sigma dx + m\omega^2 \int_0^L Z_i Z_\sigma dx\right)$$

$$-\sum_{i=1}^{n} b_{\rho i}\left(S_2\int_0^L \Phi_i^{''} Z_\sigma + \frac{EJ_\omega}{R}\int_0^L \Phi_i^{''''} Z_\sigma dx\right) = 0$$

$$\sum_{i=1}^{n} a_{\rho i}\left(\frac{EJ_\omega}{R}\int_0^L Z_i^{''''}\Phi_\sigma dx + S_2\int_0^L Z_i^{''}\Phi_\sigma dx\right)$$

$$+\sum_{i=1}^{n} b_{\rho i}\left(EJ_\omega\int_0^L \Phi_i^{''''}\Phi_\sigma dx - GJ_d\int_0^L \Phi_i^{''}\Phi_\sigma dx\right.$$

$$\left.-\left(\frac{EJ_y}{R^2}+\omega^2 J_{px}\right)\int_0^L \Phi_i\Phi_\sigma dx\right) = 0 \tag{11}$$

with $\sigma = 1\ to\ n$ and $\rho = 1\ to\ n$.

Equations (11) form a linear system of homogeneous equations with unknowns $a_{\rho i}$ and $b_{\rho i}$. For a non-trivial solution of this system, the determinant of the coefficients of the unknowns must be equal to zero, *i.e.*:

$$\left|\Delta_{ij}\right| = 0 \tag{12}$$

from which the eigenfrequencies of the bridge for coupled motion can be determined.

Eliminating the first of eqs (11) and solving the remaining equations, one can determine the constants a_i ($i = 2\ to\ n$) and b_i ($i = 1\ to\ n$), with respect to a_1 and thus, the expressions of the eigenfunctions corresponding to vertical-torsional motion of the bridge.

4.3 The orthogonality conditions

Easily, through the known process, one can determine the following orthogonality conditions for the eigenshapes determined according to the previous paragraphs 3.1 and 3.2:

4.3.1 Orthogonality conditions for the lateral motion

$$\int_0^L Y_n Y_k dx = \begin{cases} 0 & \text{for} \quad n = k \\ \Gamma_k & \text{for} \quad n \neq k \end{cases} \tag{13}$$

4.3.2 Orthogonality conditions for the coupled vertical-torsional motion

$$\int_0^L (mW_nW_k + J_{px}\Theta_n\Theta_k)dx = \begin{cases} 0 & \text{for} \quad n = k \\ \Gamma_k & \text{for} \quad n \neq k \end{cases} \tag{14}$$

5 The forced vibrating bridge

5.1 The horizontal motion

The equation of motion is:

$$EJ_z v'''' + \frac{2EJ_z}{R^2}\cdot v'' + \frac{EJ_z}{R^4}\cdot v + c_y\dot{v} + m\ddot{v} = q_y(x,t) = \bar{q}_y(x)\cdot f(t) \tag{15}$$

One can search for a solution of the form:

$$v = \sum_n Y_n(x)\cdot T_n(t) \tag{16a}$$

where $Y_n(x)$ are the eigenshapes of the bridge given by eq. (3a) and $T_n(t)$ the time functions to be determined. Introducing eq. (16a) into eq. (15) one gets:

$$EJ_z\sum_n Y_n^{''''}T_n + \frac{2EJ_z}{R^2}\sum_n Y_n^{''}T_n + \frac{EJ_z}{R^4}\sum_n Y_nT_n + c_y\sum_n Y_n\dot{T}_n + m\sum_n Y_n\ddot{T}_n = \bar{q}_y f(t)$$

Since $Y_n(x)$ satisfies the equation of free motion eq. (3a), the above expression becomes:

$$m\sum_n Y_n\ddot{T}_n + c_y\sum_n Y_n\dot{T}_n + m\sum_n \omega_{yn}^2 Y_nT_n = \bar{q}_y(x)f(t) \tag{16b}$$

Multiplying the above by Y_ρ and taking into account the orthogonality condition, one concludes to the following equation:

$$\ddot{T}_\rho(t) + \frac{c_y}{m}\dot{T}_\rho(t) + \omega_{y\rho}^2 T_\rho(t) = \frac{1}{m\int_0^L Y_\rho^2 dx}\cdot\int_0^L \bar{q}_y(x)Y_\rho(x)dx\cdot f(t) \tag{16c}$$

The solution of the above equation is given by the Duhamel's integral:

$$T_\rho(t) = \frac{\int_0^L \bar{q}_y(x)Y_\rho(x)dx}{m\bar{\omega}_{y\rho}\int_0^L Y_\rho^2 dx}\cdot\int_0^t e^{-\beta(t-\tau)}f(\tau)\cdot\sin\bar{\omega}_{y\rho}(t-\tau)\,d\tau$$

$$\text{with}: \quad \beta = \frac{c_y}{2m}, \quad \bar{\omega}_{y\rho}^2 = \omega_{y\rho}^2 - \beta^2 \tag{16d}$$

5.2 The lateral-torsional motion

The equations of motion are:

$$\left(EJ_y - \frac{EJ_\omega}{R^2}\right)w'''' + \frac{GJ_d}{R^2}\cdot w'' - \frac{EJ_y - GJ_d}{R}\cdot\phi''$$

$$-\frac{EJ_\omega}{R}\cdot\phi'''' + c_z\dot{w} + m\,\ddot{w} = \bar{q}_z(x)f_z(t) \tag{17a}$$

$$EJ_\omega\phi'''' - GJ_d\,\phi'' - \frac{EJ_y}{R^2}\cdot\phi + \frac{EJ_\omega}{R}\cdot w'''' + \frac{EJ_y - GJ_d}{R} \cdot w'' + c_\phi\dot{\phi} + J_{px}\ddot{\phi} = \bar{m}_x(x)f_\phi(t) \tag{17b}$$

One can search for a solution of the form:

$$w(x,t) = \sum_n W_n(x)\cdot P_n(t) \tag{18a}$$

$$\phi\,(x,t) = \sum_n \Theta_n(x)\cdot P_n(t) \tag{18b}$$

where W_n and Θ_n are the eigenshapes of the bridge given by eqs (10a, 10b) and $P_n(t)$ the time functions to be determined. Introducing eq. (18a, 18b) into eq. (17a, 17b) we get:

$$S_1\sum_n W_n''''P_n + \frac{GJ_d}{R^2}\sum_n W_n''P_n - S_2\sum_n \Theta_n''P_n - \frac{EJ_\omega}{R}\sum_n \Theta_n''''P_n + c_z\sum_n W_n\dot{P}_n + m\sum_n W_n\ddot{P}_n = \bar{q}_z(x)\cdot f_z(t) \tag{18c}$$

$$EJ_\omega\sum_n \Theta_n''''P_n - GJ_d\sum_n \Theta_n''P_n - \frac{EJ_y}{R^2}\sum_n \Theta_nP_n + \frac{EJ_\omega}{R}\sum_n W_n''''P_n + S_2\sum_n W_n''P_n + c_\phi\sum_n \Theta_n\dot{P}_n + J_{px}\sum_n \Theta_n\ddot{P}_n = \bar{m}_x(x)\cdot f_\phi(t) \tag{18d}$$

Since W_n and Θ_n satisfy the equations of the free motion eq. (9a, 9b), the above eqs become:

$$m\sum_n W_n\ddot{P}_n + c_z\sum_n W_n\dot{P}_n + m\sum_n \omega_{zn}^2W_nP_n = \bar{q}_z(x)\cdot f_z(t) \tag{19a}$$

$$J_{px}\sum_n \Theta_n\ddot{P}_n + c_\phi\sum_n \Theta_n\dot{P}_n + J_{px}\sum_n \omega_{zn}^2\Theta_nP_n = \bar{m}_x(x)\cdot f_\phi(t) \tag{19b}$$

Multiplying eqs (19a) by W_ρ and integrating from 0 to L, next, eqs (19b) by Θ_ρ and integrating from 0 to L, and taking into account that $c_\phi = c_zJ_{px}/m$, the above eqs become:

$$\sum_n \int_0^L mW_nW_\rho dx\cdot(\ddot{P}_n + \frac{c_z}{m}\dot{P}_n + \omega_{zn}^2P_n) = f_z(t)\int_0^L \bar{q}_z\cdot W_\rho dx \tag{20a}$$

$$\sum_n \int_0^L J_{px}\Theta_n\Theta_\rho dx\cdot(\ddot{P}_n + \frac{c_z}{m}\dot{P}_n + \omega_{zn}^2P_n) = f_\phi(t)\int_0^L \bar{m}_x\cdot\Theta_\rho dx \tag{20b}$$

The solution of the above system of equations is given by the Duhamel's integral:

$$P_\rho(t) = \frac{\int_0^L \bar{q}_zW_\rho dx}{\bar{\omega}_{z\rho}\left(m\int_0^L W_\rho^2dx + J_{px}\int_0^L \Theta_\rho^2dx\right)}\cdot\int_0^t e^{-\beta(t-\tau)}\cdot f_z(\tau)\cdot\sin\bar{\omega}_{z\rho}(t-\tau)\,d\tau + \frac{\int_0^L \bar{m}_x\Theta_\rho dx}{\bar{\omega}_{z\rho}\left(m\int_0^L W_\rho^2dx + J_{px}\int_0^L \Theta_\rho^2dx\right)}\cdot\int_0^t e^{-\beta(t-\tau)}\cdot f_\phi(\tau)\cdot\sin\bar{\omega}_{z\rho}(t-\tau)\,d\tau \tag{21}$$

where $\beta = \frac{c_z}{2m}$, $\bar{\omega}_{z\rho}^2 = \omega_{z\rho}^2 - \beta^2$.

6 The moving loads

In this section, the behavior of a curved-in-plane bridge under the action of various types of loads, moving with velocity υ is studied. In Figs (2a,b) one can see the bridge and its cross-section under the action of a concentrated load, while in Figs (2c, 2d, 2e, 2f) the different loading cases studied herein are shown.

Usually, a track cant angle φ exists on the curved parts of road bridges. This angle φ, which is important and sometimes necessary in railway bridges, has not a significant influence on road bridges, since it is always smaller than 5° (contrarily in railway bridges it may be up to 10°).

Let us examine the influence of the angle φ on the allowed safe speed υ of the moving load.

The equilibrium equation of the horizontal forces gives: $\frac{M\cdot\upsilon^2}{R} = \mu\,M\,g + M\,g\,\mathrm{Sin}\phi$, which concludes to the following inequality for the allowed speed υ:

$$\upsilon \le \sqrt{R\cdot g\cdot(\mu + \mathrm{Sin}\phi)} \tag{22}$$

The values of the coefficient of friction μ between car tires – asphalt, given by the relative manuals are:

$$\mu = 0.72 \quad \text{for dry surfaces}$$

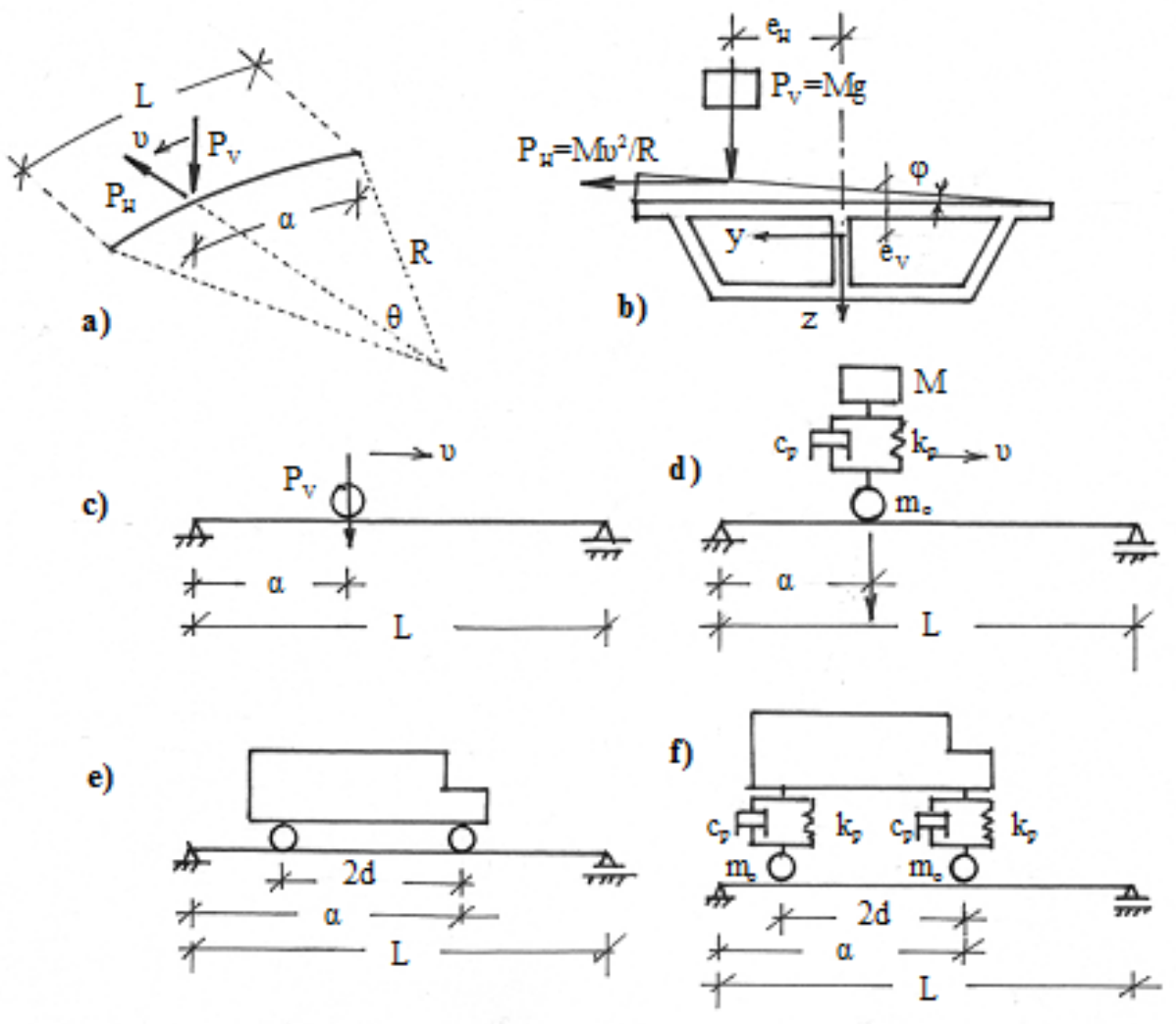

Figure 2: Bridge geometry and various cases of moving load models.

$$\mu = 0.35 \quad \text{for wet surfaces}$$

In the plots of Fig. 3, one can see the influence of angle φ on the load speed υ for both dry and wet deck surface for three characteristic radius of curvature R = 50 m (Fig. 3a), R = 100 m (Fig. 3b) and R = 150 m (Fig. 3c)

In Table 1, the allowed speeds and the achieved increase of the allowed speeds (in percentage) for $\phi = 5^\circ$ and both for dry and wet deck surface for the above chosen radius R are shown.

6.1 The concentrated moving load

In this case, the right side members of eqs (4) become:

$$q_y = \frac{M \cdot \upsilon^2}{R + e_H} \cdot \delta(x - \alpha) \tag{23a}$$

$$q_z = M \cdot g \cdot \delta(x - \alpha) \tag{23b}$$

$$m_x = \left(M \cdot g \cdot e_H + \frac{M \cdot \upsilon^2}{R + e_H} \cdot e_V \right) \cdot \delta(x - \alpha) \tag{23c}$$

where δ is the Dirac delta function and α is the position of the load P at time t.

6.1.1 The lateral motion

Introducing eq. (23a) into the right side member of eq. (15), and following the process of paragraph 4.1, one concludes to the following equation:

$$\ddot{T}_\rho + \frac{c_y}{m}\dot{T}_\rho + \omega_{y\rho}^2 T_\rho = \frac{1}{m \int_0^L Y_\rho^2 dx} \int_0^t \frac{M\upsilon^2}{R + e_H} Y_\rho(x)\delta(x - \alpha)dx$$

Table 1: Maximum speeds for various R, φ and deck surface conditions.

	R= 50 m			R= 100 m			R= 150 m		
φ	5°	0°	%	5°	0°	%	5°	0°	%
dry	20.25	18.80	7.7	28.80	26.80	7.4	35.10	32.90	6.6
wet	15.10	13.20	14.4	21.30	18.65	14.3	26.10	22.90	13.9

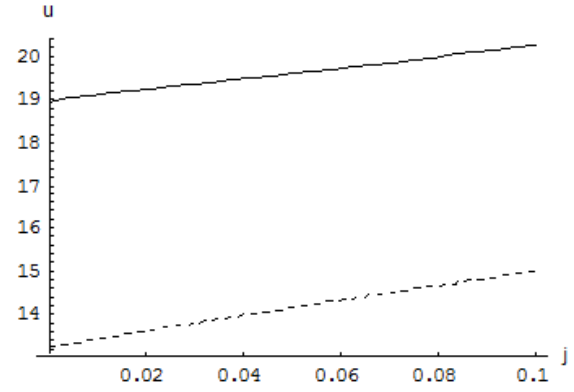

(a)

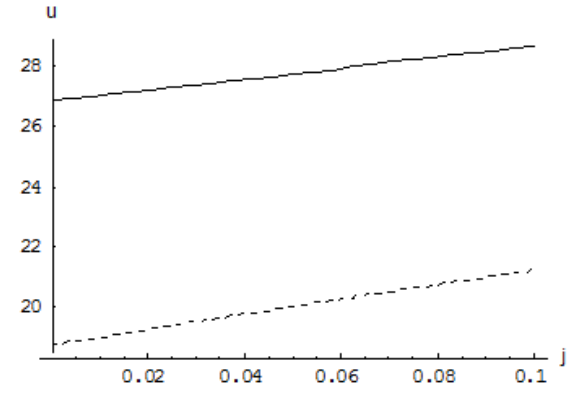

(b)

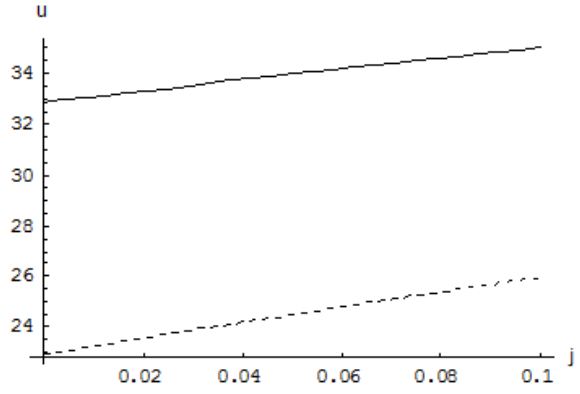

(c)

Figure 3: The influence of track cant angle φ on the allowed speed υ for various R.

$$= \frac{M\upsilon^2}{m(R+e_H)\int_0^L Y_\rho^2 dx} Y_\rho(\alpha)$$

or finally:

$$\ddot{T}_\rho + \frac{c_y}{m}\dot{T}_\rho + \omega_{y\rho}^2 T_\rho = \frac{M\upsilon^2}{m(R+e_H)\int_0^L Y_\rho^2 dx} Y_\rho(\upsilon t),$$

which has the solution:

$$T_\rho = \frac{M\upsilon^2}{m(R+e_H)\bar{\omega}_{y\rho}\int_0^L Y_\rho^2 dx} \cdot \int_0^t e^{-\beta(t-\tau)} Y_\rho(\upsilon\tau)\mathrm{Sin}\bar{\omega}_{y\rho}(t-\tau)\,d\tau \qquad (24)$$

with β and $\bar{\omega}_{y\rho}$ from eq. (16).

6.1.2 The vertical-torsional motion

Introducing eqs (23b, 23c) into the right side members of eqs (20a, 20b) and following the process of paragraph 4.2, one concludes to the following equation:

$$\ddot{P}_\rho + \frac{c_z}{m}\dot{P}_\rho + \omega_{z\rho}^2 P_\rho = \frac{M\cdot g\cdot Z_\rho(\upsilon t) + \left(M\cdot g\cdot e_H + \frac{M\upsilon^2}{R+e_H}e_V\right)\Theta_\rho(\upsilon t)}{m\int_0^L Z_\rho^2 dx + J_{px}\int_0^L \Theta_\rho^2 dx}$$

which has the solution:

$$P_\rho = \frac{M\cdot g\cdot Z_\rho(\upsilon t)}{\left(m\int_0^L Z_\rho^2 dx + J_{px}\int_0^L \Theta_\rho^2 dx\right)}\int_0^L e^{-\beta(t-\tau)}\cdot Z_\rho(\upsilon\tau) \cdot \mathrm{Sin}\bar{\omega}_{z\rho}(t-\tau)\,d\tau + \frac{M\cdot g\cdot e_H + \frac{M\upsilon^2}{R+e_H}e_V}{\left(m\int_0^L Z_\rho^2 dx + J_{px}\int_0^L \Theta_\rho^2 dx\right)} \cdot \int_0^L e^{-\beta(t-\tau)}\cdot\Theta_\rho(\upsilon\tau)\cdot\mathrm{Sin}\bar{\omega}_{z\rho}(t-\tau)\,d\tau \qquad (25)$$

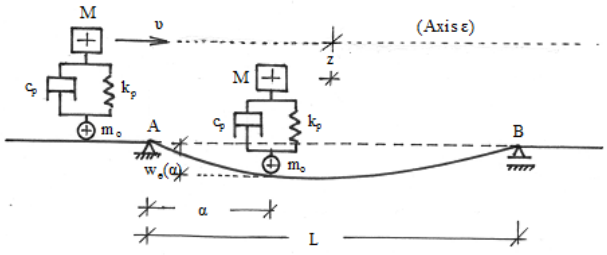

Figure 4: The damped mass-load.

6.2 The moving damped mass-load

Let us consider next the mass-load M of Fig. 4, moving with a constant velocity υ and supported through a suspension system on wheels with mass m_o.

This system is composed of an elastic spring with constant k_p and a damper with constant c_p.

When the load, *i.e.*, the system of masses M and m_o is on the left end of the bridge (at $t = 0$), the spring is statically deformed by $\frac{P}{k_p} = \frac{Mg}{k_p}$.

Considering axis (ϵ) as the reference system for measuring the motion of the mass M (Fig. 4) and applying the Newton's second law, one obtains: $M\ddot{z} = P - k_p\left(\frac{P}{k_p} + z - w(\alpha)\right) - c_p[\dot{z} - \dot{w}(\alpha)]$ or

$$M\ddot{z} + c_p\dot{z} + k_p z = k_p w_e(\alpha) + c_p\dot{w}_e(\alpha)$$
$$\text{where :} \quad w_e(\alpha) = w(\alpha) + e_H\phi(\alpha) \tag{26a}$$

and φ is the angle at $x = \alpha$ and e_H from Fig. 2. The above relation can also be written as follows:

$$\ddot{z} + 2\beta_p\dot{z} + \omega_p^2 z = F(t) \tag{26b}$$

$$\text{where :} \quad F(t) = \omega_p^2[w(\alpha) + e_H\phi(\alpha)] + 2\beta_p[\dot{w}(\alpha) + e_H\dot{\phi}(\alpha)]$$
$$\beta_p = \frac{c_p}{2M}, \quad \omega_p^2 = \frac{k_p}{M} \tag{26c}$$

The solution of the above differential equation (26b) is given by the following integral:

$$z(t) = \frac{1}{\bar{\omega}_p}\int_0^t e^{-\beta_p(t-\tau)}F(\tau)\cdot\sin\bar{\omega}_p(t-\tau)\,d\tau \tag{26d}$$

$$\text{with :} \quad \bar{\omega}_p = \sqrt{\omega_p^2 - \beta^2} \tag{26e}$$

Applying the Leibnitz formula, according to which the function $f(x) = \int_{a(x)}^{b(x)} R(x,t)dt$, can be differentiated as follows: $\frac{df(x)}{dx} = R(x,b(x))\frac{db(x)}{dx} - R(x,a(x))\frac{da(x)}{dx} + \int_{a(x)}^{b(x)}\frac{\partial R(x,t)}{\partial x}dt$, equation (26d) gives successively:

$$\dot{z}(t) = \frac{1}{\bar{\omega}_p}\int_0^t e^{-\beta(t-\tau)}F(\tau)\,[\bar{\omega}_p\cos\bar{\omega}_p(t-\tau) - \beta_p\sin\bar{\omega}_p(t-\tau)]\,d\tau \tag{27a}$$

$$\ddot{z}(t) = F(t) + \frac{1}{\bar{\omega}_p}\int_0^t e^{-\beta(t-\tau)}F(\tau)\,[(\beta_p^2 - \bar{\omega}_p^2)\sin\bar{\omega}_p(t-\tau) - 2\beta_p\bar{\omega}_p\cos\bar{\omega}_p(t-\tau)]\,d\tau \tag{27b}$$

Therefore, the right side members of eqs (1) become:

$$q_y = \frac{M\upsilon^2}{R + e_H}\cdot\delta(x-\alpha) \tag{28a}$$

$$q_z = \left\{M(g-\ddot{z}) + m_o[g - \ddot{w}(\alpha) - e_H\ddot{\phi}(\alpha)]\right\}\cdot\delta(x-\alpha) \tag{28b}$$

$$m_x = \left\{M(g-\ddot{z}) + m_o[g - \ddot{w}(\alpha) - e_H\ddot{\phi}(\alpha)]\right\}\cdot e_H\cdot\delta(x-\alpha) + \frac{M\upsilon^2}{R + e_H}\cdot e_V\cdot\delta(x-\alpha) \tag{28c}$$

6.2.1 The lateral motion

Introducing eq (28a) into the right side member of eq. (15), one concludes to the solution of eq. (24).

6.2.2 The vertical-torsional motion

Introducing eqs (28b, 28c) into the right side members of eqs (17a, 17b), one concludes to the following equations:

$$S_1 w'''' + \frac{GJ_d}{R^2}w'' - S_2\phi'' - \frac{EJ_\omega}{R}\phi'''' + c_z\dot{w} + m\ddot{w} = \left\{(M+m_o)g - M\ddot{z} - m_o[\ddot{w}(\alpha) + e_H\ddot{\phi}(\alpha)]\right\}\cdot\delta(x-\alpha) \tag{29a}$$

$$EJ_\omega\phi'''' - GJ_d\phi'' - \frac{EJ_y}{R^2}\phi + \frac{EJ_\omega}{R}w'''' + S_2 w'' + c_\phi\dot{\phi} + J_{px}\ddot{\phi} = \left[\left\{(M+m_o)g - M\ddot{z} - m_o[\ddot{w}(\alpha) + e_H\ddot{\phi}(\alpha)]\right\}\cdot e_H + \frac{M\upsilon^2}{R+e_H}\cdot e_V\right]\cdot\delta(x-\alpha) \tag{29b}$$

One can search for a solution in the form:

$$w(x,t) = \sum_n W_n(x)T_n(t) \tag{29c}$$

$$\phi(x,t) = \sum_n \Theta_n(x) T_n(t) \tag{29d}$$

where W_n and Θ_n are the shape functions, according to §3.2.

Following the procedure described in the preceding sections, the following differential equation for the time function $T_\rho(t)$ is obtained:

$$\begin{aligned}
\ddot{T}_\rho + \frac{c_z}{m}\dot{T}_\rho + \omega_\rho^2 T_\rho = {} & \frac{1}{m\int_0^L W_\rho^2 dx + J_{px}\int_0^L \Theta_\rho^2 dx}\Bigg\{(M+m_o) \\
& \cdot g \cdot W_\rho(\upsilon t) - M W_\rho(\upsilon t)\sum_n (R_n(\upsilon t)[\omega_p^2 T_n(t) + 2\beta_p \dot{T}_n(t)]) \\
& - \frac{M}{\bar{\omega}_\rho}\Bigg[\omega_p^2 W_\rho(\upsilon t)\sum_n R_n(\upsilon t) Q_{1n}(t) \\
& + 2\beta_p W_\rho(\upsilon t)\sum_n R_n(\upsilon t) Q_{2n}(t)\Bigg] \\
& - m_o W_\rho(\upsilon t)\sum_n R_n(\upsilon t)\ddot{T}(t) \\
& - M e_H \Theta_\rho(\upsilon t)\sum_n (R_n(\upsilon t)[\omega_p^2 T_n(t) + 2\beta_p \dot{T}_n(t)]) \\
& - \frac{M e_H}{\bar{\omega}_\rho}\Bigg[\omega_p^2 \Theta_\rho(\upsilon t)\sum_n R_n(\upsilon t) Q_{1n}(t) \\
& + 2\beta_p \Theta_\rho(\upsilon t)\sum_n R_n(\upsilon t) Q_{2n}(t)\Bigg] + \frac{M\upsilon^2}{R+e_H}\cdot e_V \Theta_\rho(\upsilon t)\Bigg\}
\end{aligned} \tag{30a}$$

where:

$$\begin{aligned}
R_n(x) &= W_n(x) + e_H \Theta_n(x) \\
Q_{1n}(t) &= \int_0^t T_n(\tau)\cdot e^{-\beta(t-\tau)}\Xi(\tau)d\tau \\
Q_{2n}(t) &= \int_0^t \dot{T}_n(\tau)\cdot e^{-\beta(t-\tau)}\Xi(\tau)d\tau \\
\Xi(\tau) &= e^{-\beta(t-\tau)}\left[(\beta_p^2 - \bar{\omega}_p^2)\sin\bar{\omega}_\rho(t-\tau)\right. \\
&\quad \left. -2\beta_p\bar{\omega}_\rho\cos\bar{\omega}_\rho(t-\tau)\right]
\end{aligned} \tag{30b}$$

Clearly, a closed form solution of eq. (30a) is not possible. However, one can seek approximate solutions based on previous pertinent works (Kounadis [37], Michaltsos [16]). A first approximate solution of eq. (30a), is obtained by considering as loading the force $P = Mg$, that leads to eqs (25). Introducing the known $P_\rho(t)$ instead of $T_n(t)$ in the right side member of eq. (30a), one can determine its solution according to Duhamel's integral.

6.3 The moving vehicle

Let us consider next the vehicle of Fig. 5b, moving on the curved bridge (see Fig. 5a) with constant speed υ. This case of loading can be easily solved following the above procedure with external loads:

$$\begin{aligned}
q_y = {} & \left(\frac{M\cdot\upsilon^2}{4(R+e_H-b)} + \frac{M\cdot\upsilon^2}{4(R+e_H+b)}\right)\cdot\delta(x-\alpha) \\
& + \left(\frac{M\cdot\upsilon^2}{4(R+e_H-b)} + \frac{M\cdot\upsilon^2}{4(R+e_H+b)}\right)\cdot\delta(x-\alpha+2d)
\end{aligned} \tag{31a}$$

$$q_z = \frac{M\cdot g}{2}\cdot\delta(x-\alpha) + \frac{M\cdot g}{2}\cdot\delta(x-\alpha+2d) \tag{31b}$$

$$\begin{aligned}
m_x = {} & \left(\frac{M\cdot g}{4} + \frac{F_c e_V}{4b}\right)(e_H+b)\cdot\delta(x-\alpha) \\
& + \left(\frac{M\cdot g}{4} - \frac{F_c e_V}{4b}\right)(e_H-b)\cdot\delta(x-\alpha) \\
& + \left(\frac{M\cdot g}{4} + \frac{F_c e_V}{4b}\right)(e_H+b)\cdot\delta(x-\alpha+2d) \\
& + \left(\frac{M\cdot g}{4} - \frac{F_c e_V}{4b}\right)(e_H-b)\cdot\delta(x-\alpha+2d)
\end{aligned} \tag{31c}$$

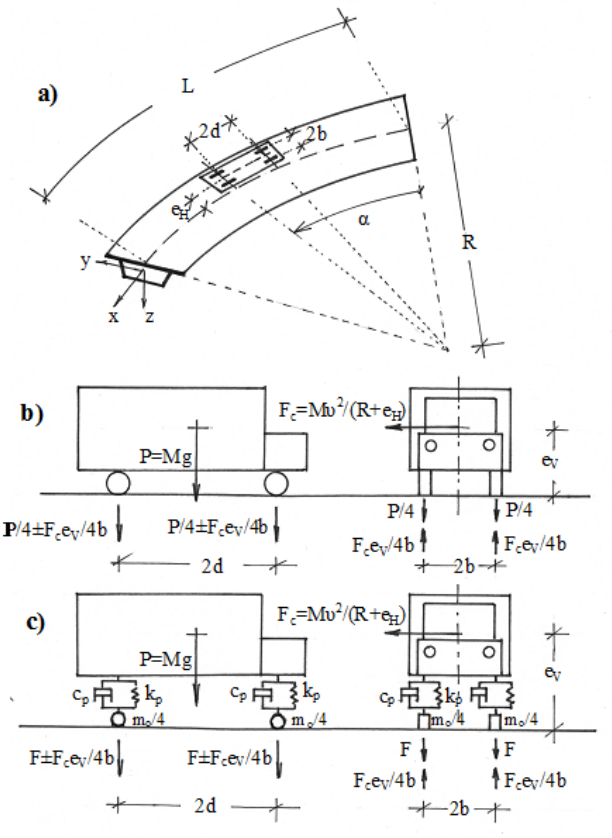

Figure 5: The curved bridge (a), the moving vehicle (b) and the damped vehicle (c).

The first members of eqs (31a, 31b), and the first two of eqs (31c) are valid for $0 \le t \le L/\upsilon$, while the second members of eqs (31a, 31b), and the third and fourth members of eqs (31c) are valid for $2d/\upsilon \le t \le (L+2d)/\upsilon$.

6.3.1 The lateral motion

Introducing eq. (31a) into the right side member of eq. (15), and following the process of §4.1, one concludes to the following equation:

$$T_\rho = \frac{Q_y}{m\bar{\omega}_{y\rho}\int_0^L Y_\rho^2 dx}\left\{\left(\int_0^t e^{-\beta(t-\tau)}Y_\rho(\upsilon\tau)\mathrm{Sin}\bar{\omega}_{y\rho}(t-\tau)\,d\tau\right)\cdot\left[1-H\left(1-\frac{L}{\upsilon}\right)\right]+\left(\int_0^t e^{-\beta(t-\tau)}Y_\rho(\upsilon\tau-2d)\cdot\mathrm{Sin}\bar{\omega}_{y\rho}(t-\tau)\,d\tau\right)\cdot H\left(1-\frac{2d}{\upsilon}\right)\right\} \tag{32a}$$

$$\text{with}\quad \mathrm{Q_y} = \frac{M\upsilon^2}{4\cdot(R+e_H-b)}+\frac{M\upsilon^2}{4\cdot(R+e_H+b)} \tag{32b}$$

where H is the Heaviside unit function.

6.3.2 The vertical-torsional motion

Introducing eqs (31b, 31c) into the right side members of eqs (17a, 17b) and following the known process, one concludes to the following equation:

$$P_\rho(t) = \frac{1}{K_\rho}[R_{1\rho}(t)+Q_{1\rho}(t)+Q_{3\rho}(t)] + \frac{1}{K_\rho}[R_{2\rho}(t)+Q_{2\rho}(t)+Q_{4\rho}(t)] \tag{33a}$$

where:

$$K_\rho = \bar{\omega}_{z\rho}\left(m\int_0^L Z_\rho^2 dx + J_{px}\int_0^L \Theta_\rho^2 dx\right)$$

$$R_{1\rho}(t) = \frac{Mg}{2}\left(\int_0^L e^{-\beta(t-\tau)}Z_\rho(\upsilon\tau)\,\mathrm{Sin}\bar{\omega}_{z\rho}(t-\tau)\,d\tau\right)\cdot\left(1-H\left(t-\frac{L}{\upsilon}\right)\right)$$

$$R_{2\rho}(t) = R_{1\rho}\left(t-\frac{2d}{\upsilon}\right)H\left(t-\frac{2d}{\upsilon}\right)$$

$$Q_{1\rho}(t) = \left(\frac{Mg}{4}+\frac{F_c e_V}{4b}\right)(e_H+b)\cdot\left(\int_0^L e^{-\beta(t-\tau)}\Phi_\rho(\upsilon\tau)\,\mathrm{Sin}\bar{\omega}_{z\rho}(t-\tau)\,d\tau\right)\cdot\left(1-H\left(t-\frac{L}{\upsilon}\right)\right)$$

$$Q_{2\rho}(t) = Q_{1\rho}\left(t-\frac{2d}{\upsilon}\right)H\left(t-\frac{2d}{\upsilon}\right)$$

$$Q_{3\rho}(t) = \left(\frac{Mg}{4}-\frac{F_c e_V}{4b}\right)(e_H-b)\cdot\left(\int_0^L e^{-\beta(t-\tau)}\Phi_\rho(\upsilon\tau)\,\mathrm{Sin}\bar{\omega}_{z\rho}(t-\tau)\,d\tau\right)\cdot\left(1-H\left(t-\frac{L}{\upsilon}\right)\right)$$

$$Q_{4\rho}(t) = Q_{3\rho}\left(t-\frac{2d}{\upsilon}\right)H\left(t-\frac{2d}{\upsilon}\right) \tag{33b}$$

where H is the Heaviside's unit function.

6.4 The damped vehicle

Consider the vehicle of Fig. 5c, moving on the bridge with constant speed υ. This case of loading can be easily solved following the known procedure with external loads:

$$q_y = \left(\frac{M\cdot\upsilon^2}{4(R+e_H-b)}+\frac{M\cdot\upsilon^2}{4(R+e_H+b)}\right)\cdot\delta(x-\alpha) + \left(\frac{M\cdot\upsilon^2}{4(R+e_H-b)}+\frac{M\cdot\upsilon^2}{4(R+e_H+b)}\right)\cdot\delta(x-\alpha+2d) \tag{34a}$$

$$q_z = 2\cdot F\cdot\delta(x-\alpha)+2\cdot F\cdot\delta(x-\alpha+2d) \tag{34b}$$

$$m_x = \left(F+\frac{F_c e_V}{4b}\right)(e_H+b)\cdot\delta(x-\alpha)+\left(F-\frac{F_c e_V}{4b}\right)\cdot(e_H-b)\cdot\delta(x-\alpha)+\left(F+\frac{F_c e_V}{4b}\right)(e_H+b)\cdot\delta(x-\alpha+2d)+\left(F-\frac{F_c e_V}{4b}\right)(e_H-b)\cdot\delta(x-\alpha+2d) \tag{34c}$$

where:

$$F = \frac{1}{4}\{M(g-\ddot{z})+m_o[g-\ddot{w}(\alpha)-e_H\ddot{\phi}(\alpha)]\}$$

$$F_c = \frac{M\upsilon^2}{R+e_H} \tag{34d}$$

The first members of eqs (34a, 34b), and the first two of eqs (34c) are valid for $0 \le t \le L/\upsilon$, while the second members of eqs (34a, 34b), and the third and fourth members of eq. (34c) are valid for $2d/\upsilon \le t \le (L+2d)/\upsilon$.

6.4.1 The lateral motion

Introducing eq. (34a) into the right side member of eq. (15) and following the process of §4.1 one concludes to the solution of eqs (32a) and (32b).

6.4.2 The vertical-torsional motion

Introducing eqs (34b, 34c) into the right side members of eqs (17a, 17b) and following the known process, one concludes to the following equation:

$$P_\rho(t) = \frac{1}{K_\rho}[R_{1\rho}(t) + Q_{1\rho}(t) + Q_{3\rho}(t)] + \frac{1}{K_\rho}[R_{2\rho}(t) + Q_{2\rho}(t) + Q_{4\rho}(t)] \tag{35a}$$

where:

$$K_\rho = \bar{\omega}_{z\rho}\left(m\int_0^L Z_\rho^2 dx + J_{px}\int_0^L \Theta_\rho^2 dx\right)$$

$$R_{1\rho}(t) = 2\cdot F\cdot\left(\int_0^L e^{-\beta(t-\tau)} Z_\rho(\upsilon\tau)\,\mathrm{Sin}\bar{\omega}_{z\rho}(t-\tau)\,d\tau\right)\cdot\left(1 - H\left(t-\frac{L}{\upsilon}\right)\right)$$

$$R_{2\rho}(t) = R_{1\rho}\left(t-\frac{2d}{\upsilon}\right)H\left(t-\frac{2d}{\upsilon}\right)$$

$$Q_{1\rho}(t) = \left(F + \frac{F_c e_V}{4b}\right)(e_H + b)\cdot\left(\int_0^L e^{-\beta(t-\tau)}\Phi_\rho(\upsilon\tau)\,\mathrm{Sin}\bar{\omega}_{z\rho}(t-\tau)\,d\tau\right)\cdot\left(1 - H\left(t-\frac{L}{\upsilon}\right)\right)$$

$$Q_{2\rho}(t) = Q_{1\rho}\left(t-\frac{2d}{\upsilon}\right)H\left(t-\frac{2d}{\upsilon}\right)$$

$$Q_{3\rho}(t) = \left(F - \frac{F_c e_V}{4b}\right)(e_H - b)\cdot\left(\int_0^L e^{-\beta(t-\tau)}\Phi_\rho(\upsilon\tau)\,\mathrm{Sin}\bar{\omega}_{z\rho}(t-\tau)\,d\tau\right)\cdot\left(1 - H\left(t-\frac{L}{\upsilon}\right)\right)$$

$$Q_{4\rho}(t) = Q_{3\rho}\left(t-\frac{2d}{\upsilon}\right)H\left(t-\frac{2d}{\upsilon}\right) \tag{35b}$$

and H is the Heaviside unit function.

7 Numerical results and discussion

Let us consider a bridge, curved-in-plane, with length L = 60 m (see Fig. 4). The bridge is made from structural steel (isotropic and homogeneous material) with modulus of elasticity $E = 2,1 \times 10^8$ kN/m^2, shear modulus $G = 0,8 \times 10^8$ kN/m^2, moments of inertia $J_y = 0,50$ m^4, $J_z = 8,00$ m^4, torsional constant $J_d = 0,50$ m^4, warping constant $J_\omega = 0,25$ m^6, mass per unit length m = 1200 kg/m and mass moment of inertia J_{px} = 10200 kg·m^2. Three characteristic radius of curvature are considered: R = 50 m, R = 100 m, and R = 150 m.

We will study the dynamic behavior of the bridge under the action of:

(a) A concentrated moving load with speed υ and magnitude $P = M \cdot g$ and M = 4000 kg.
(b) A concentrated damped mass-load moving with speed υ and magnitude $P = M \cdot g$.
(c) A vehicle with dimensions $2d \cdot 2b$, whose the tires are considered as concentrated loads, and of a consequence of two concentrated loads spaced at 2d with magnitude $P_1 = P_2 = M \cdot g/2$.
(d) A vehicle with dimensions $2d \cdot 2b$, having mass M and mass of its four tires m_o = 40 kg, and damping system with k_p = 10000 dN/m, c_p = 500 dN·s/m.

According to the results of Table 1, the studied speeds must be less than υ = 35 m/sec.

7.1 The concentrated moving load

7.1.1 The lateral motion

- Influence of the radius of curvature

The plots of Fig. 6 show the lateral vibrations of the middle of the bridge (at $x = L/2$) for speeds υ = 10 m/s (Fig. 6a), υ = 20 m/s (Fig. 6b), and υ = 30 m/s (Fig. 6c) and various values of radius of curvature.

As expected, it is observed that for small R the developed deflections are much higher than the ones for big R. These differences amount to:

about 150% for 100 < R < 150 m
about 250% for 50 < R < 100 m
about 400% for 50 < R < 150 m

These percentage differences are slightly affected by the value of the speed υ.

- Influence of the eccentricity

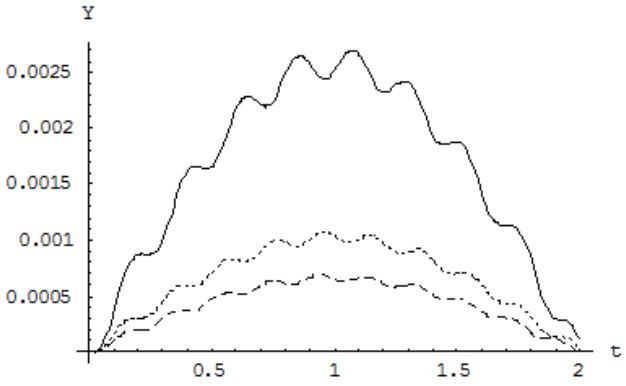

(a) $\upsilon = 10$ m/s

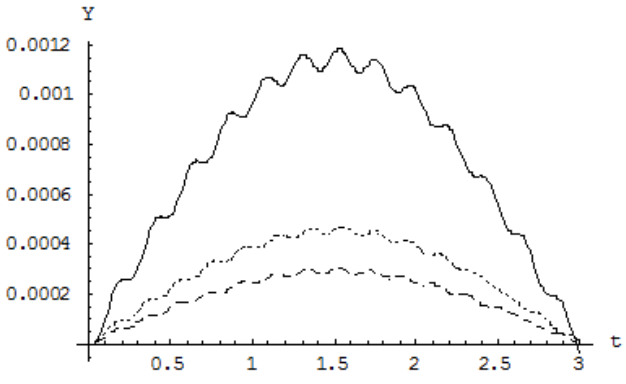

(b) $\upsilon = 20$ m/s

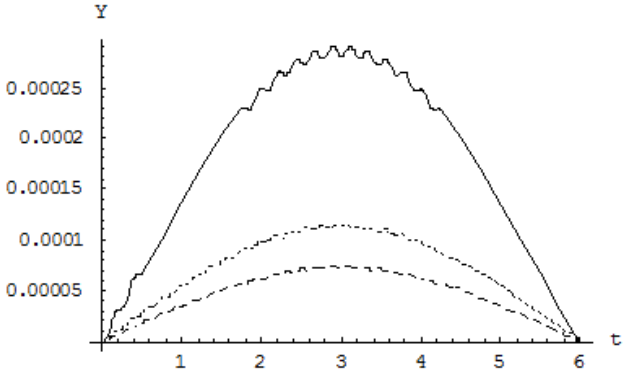

(c) $\upsilon = 30$ m/s

Figure 6: The influence of the radius of curvature for various values of υ: ___ $R = 50$ m, ... $R = 100$ m, - - - $R = 150$ m.

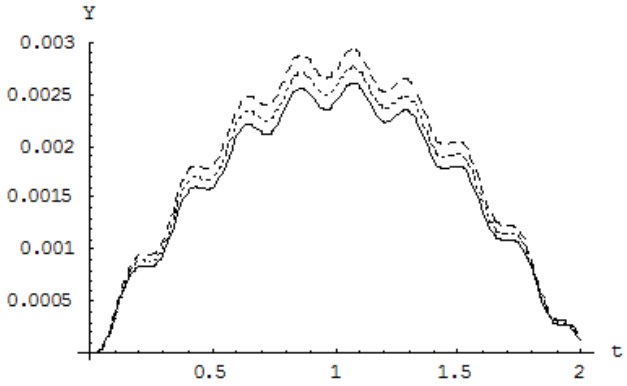

(a) $R = 50$ m

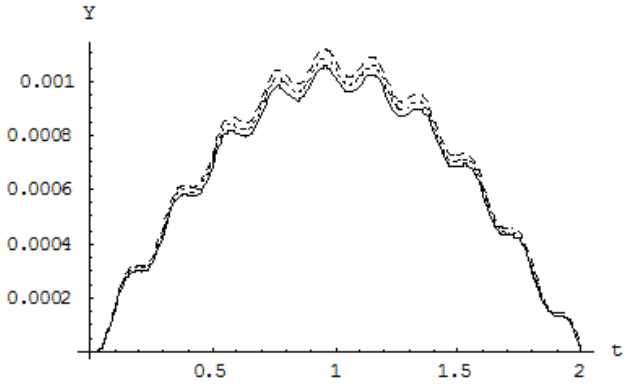

(b) $R = 100$ m

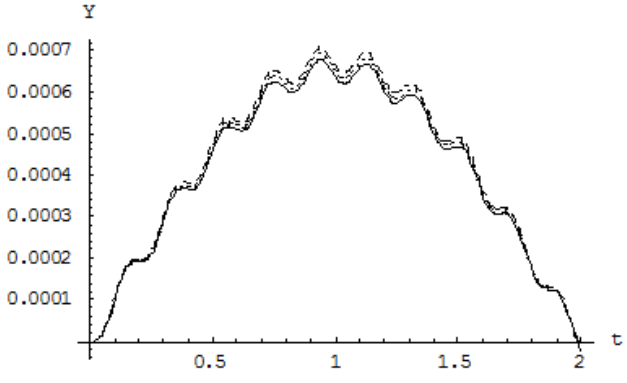

(c) $R = 150$ m

Figure 7: The influence of the eccentricity for $\upsilon = 30$ m/s and various values of R: ___ $e_H = 3$ m, ... $e_H = 0$ m, - - - $e_H = -3$ m.

The plots of Fig. 7 show the lateral vibrations of the middle of the bridge (at $x = L/2$) for $\upsilon = 30$ m/s, eccentricities $e_H = 3$ m, $e_H = 0$ m, $e_H = -3$ m, and various radii of curvature.

From these plots, one can see that as R increases, the influence of the eccentricity e_H on the bridge's deflections decreases. For $R = 50$ m and $\upsilon = 30$ m/s the difference between $e_H = 3$ and $e_h = -3$ amounts to about 15%, while for $R = 150$ m and $\upsilon = 30$ m/s the difference between $e_H = 3$ and $e_h = -3$ amounts to about 3%.

- Influence of the speed

Finally, in Fig. 8 one can see the deflections of the middle of the bridge for $R = 50$ m, $e_H = 0$ and various values of speed.

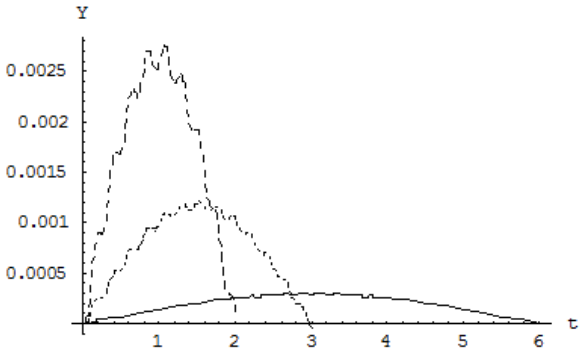

Figure 8: The influence of the speed for $R = 50$ m, $e_H = 0$ m and $\upsilon = 10$ m/s (___), $\upsilon = 20$ m/s (.....), $\upsilon = 30$ m/s (- - -).

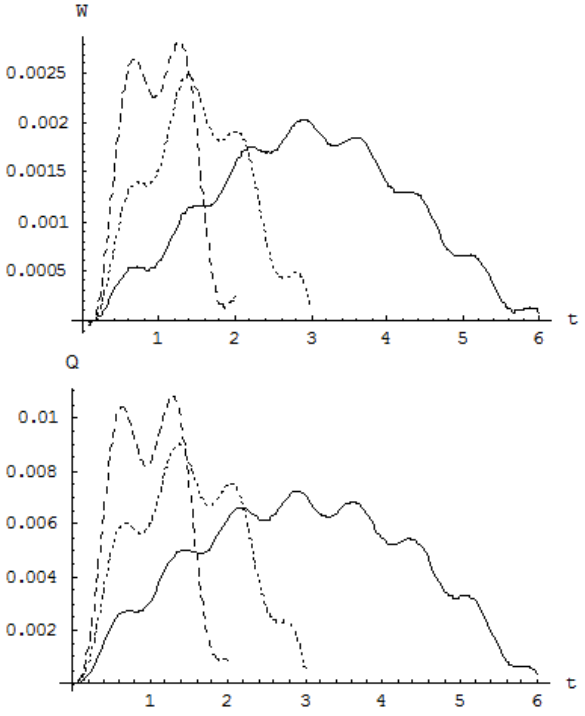

Figure 9: The influence of the speed for $R = 50$ m, $e_H = 3$ m, $e_V = 1.20$ m, and $\upsilon = 10$ m/s (___), $\upsilon = 20$ m/s (.....), $\upsilon = 30$ m/s (- - -).

7.1.2 The vertical-torsional motion

- Influence of the speed

The plots of Fig. 9 show the vertical-torsional vibrations of the middle of the bridge (at $x = L/2$) for $R = 50$ m, eccentricity $e_H = 3$ m, and $e_V = 1.20$ m.

The plots of Fig. 10 show the vertical-torsional vibrations of the middle of the bridge (at $x = L/2$) for $R = 100$ m, eccentricity $e_H = 3$ m, and $e_V = 1.20$ m.

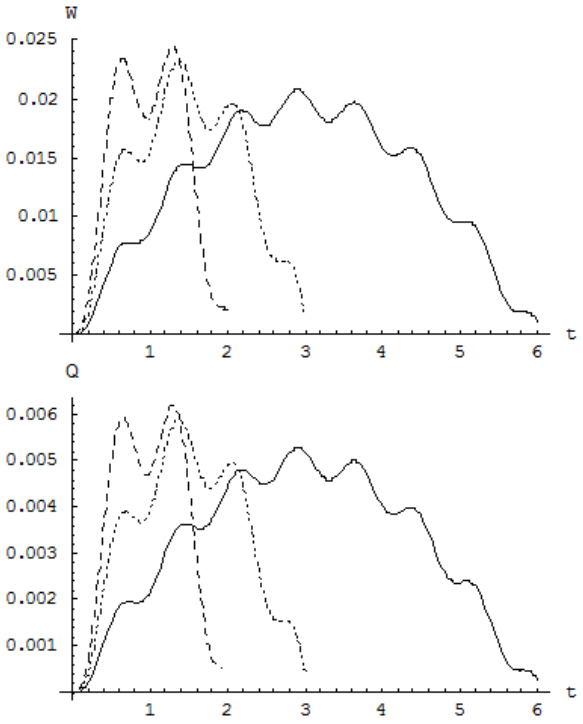

Figure 10: The influence of the speed for $R = 100$ m, $e_H = 3$ m, $e_V = 1.20$ m, and $\upsilon = 10$ m/s (___), $\upsilon = 20$ m/s (.....), $\upsilon = 30$ m/s (- - -).

The plots of Fig. 11 show the vertical-torsional vibrations of the middle of the bridge (at $x = L/2$) for $R = 150$ m, eccentricity $e_H = 3$ m, and $e_V = 1.20$ m.

From the above plots, one can ascertain that for both deformations (deflection and torsion), the influence of the speed is higher in bridges with small radius of curvature than in bridges with big radius of curvature. For the cases studied, this influence amounts to about 60–70% for $R = 50$ m decreasing to about 10–20% for $R = 150$ m.

- Influence of the radius of curvature

The plots of Fig. 12 show the vertical-torsional motion of the middle of the bridge (at $x = L/2$) for speed $\upsilon = 20$ m/s, $e_H = 1.50$ m, $e_V = 1.20$ m, and various radii of curvature.

- Influence of the eccentricity

The plots of Fig. 13 show the vertical-torsional vibrations of the middle of the bridge (at $x = L/2$) for $R = 50$ m, $\upsilon = 30$ m/s, and various values of eccentricity.

The plots of Fig. 14 show the vertical-torsional vibrations of the middle of the bridge (at $x = L/2$) for $R = 100$ m, $\upsilon = 30$ m/s, and various values of eccentricity.

The plots of Fig. 15 show the vertical-torsional vibrations of the middle of the bridge (at $x = L/2$) for $R = 150$ m, $\upsilon = 30$ m/s, and various values of eccentricity.

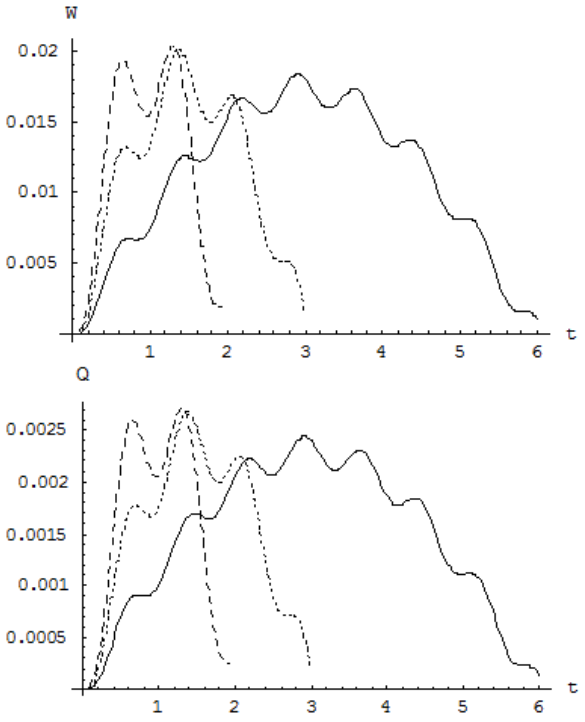

Figure 11: The influence of the speed for $R = 150$ m, $e_H = 3$ m, $e_V = 1.20$ m, and $\upsilon = 10$ m/s (___), $\upsilon = 20$ m/s (.....), $\upsilon = 30$ m/s (- - -).

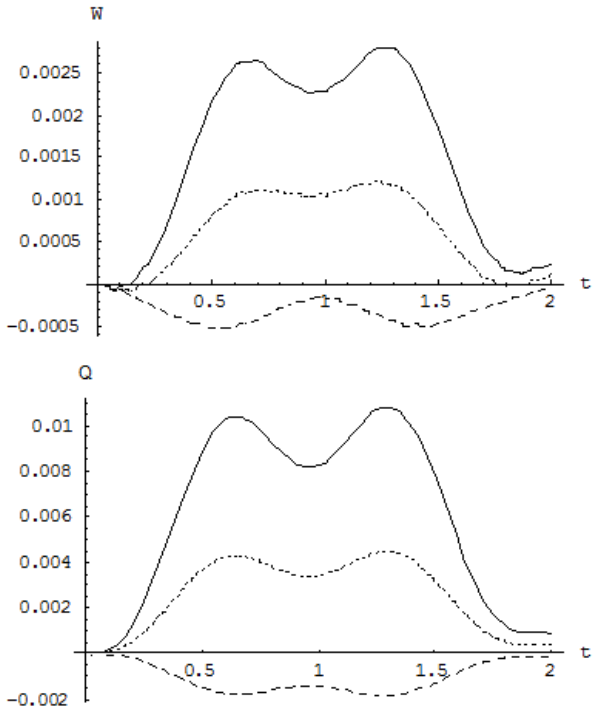

Figure 13: The influence of the eccentricity for $\upsilon = 30$ m/s, $R = 50$ m, and ___ $e_H = 3$ m, ... $e_H = 0$ m, - - - $e_H = -3$ m.

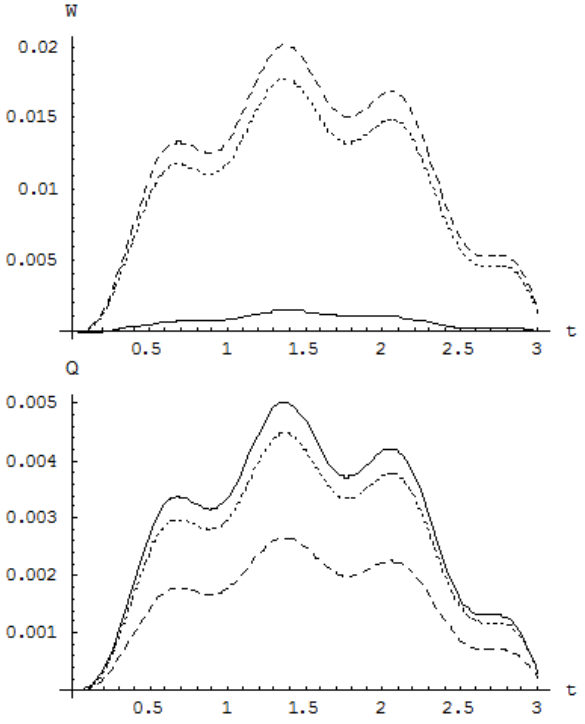

Figure 12: The influence of the radius of curvature for $\upsilon = 20$ m/s, $e_H = 1.5$ m, $e_V = 1.2$ m and $R = 50$ m (___), $R = 100$ m (.....), $R = 150$ m (- - -).

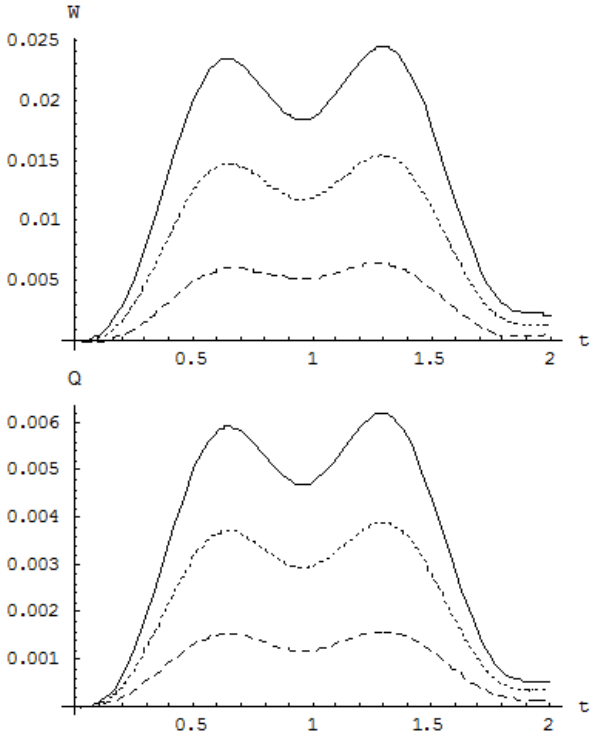

Figure 14: The influence of the eccentricity for $\upsilon = 30$ m/s, $R = 100$ m, and ___ $e_H = 3$ m, ... $e_H = 0$ m, - - - $e_H = -3$ m.

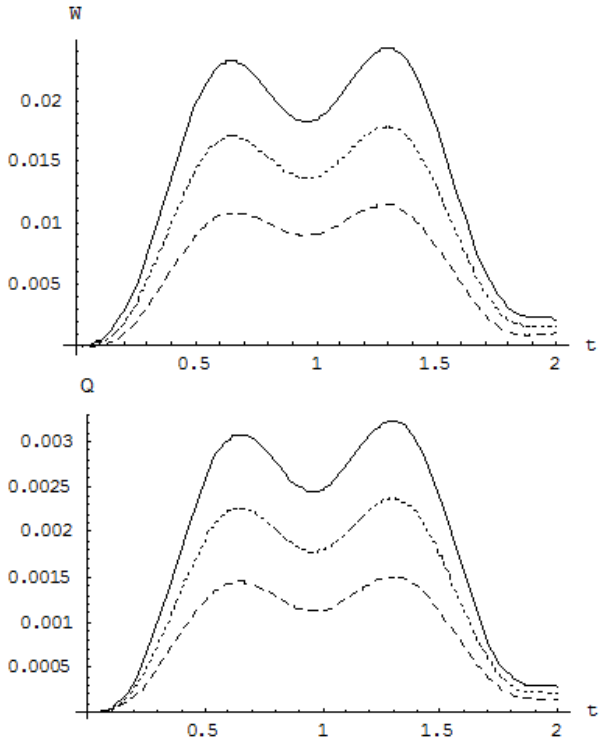

Figure 15: The influence of the eccentricity for $\upsilon = 30$ m/s, $R = 150$ m, and ___ $e_H = 3$ m, ... $e_H = 0$ m, - - - $e_H = -3$ m.

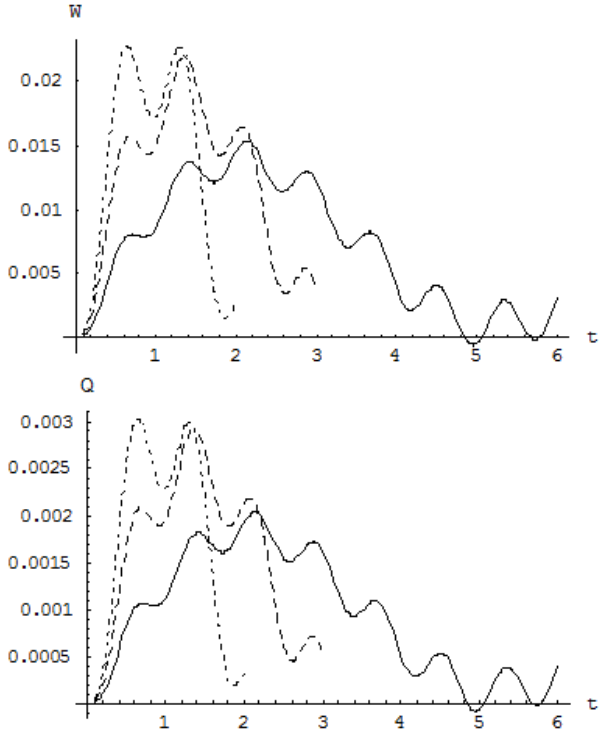

Figure 16: The influence of the vehicle's speed for $R = 150$ m, $e_H = 3$ m and $\upsilon = 10$ m/s (__), $\upsilon = 20$ m/s (_ _) and $\upsilon = 30$ m/s (- - -).

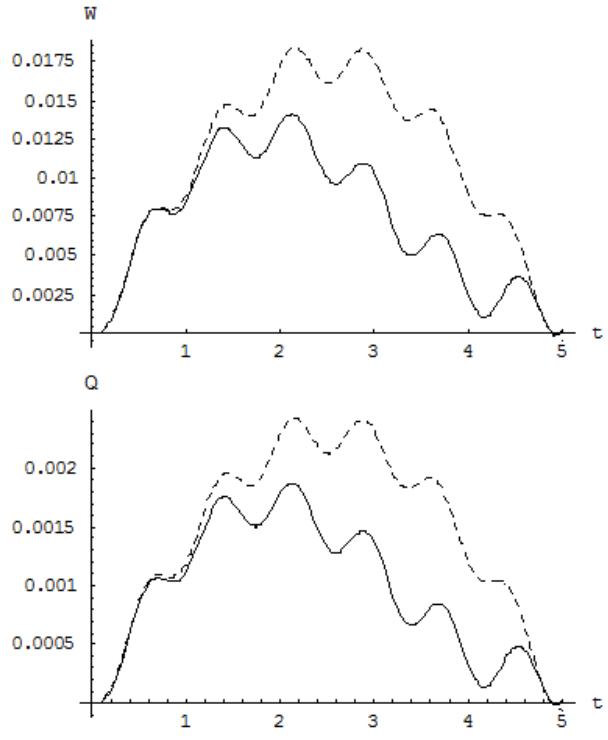

Figure 17: The influence of the load model for $R = 150$ m and $\upsilon = 10$ m/s and (- - -) Concentrated load $P = Mg$, (___) Damped mass-load M.

From the plots of Fig. 13 and for $e_H = -3$, we observe that both deformations (deflection and torsion) are negative. This was expected for the rotation angle, but not for the deflection. However, this deflection is referred to the axis of the cross-section, while the deflection of the point where the load is applied is: $-0.0005 + (-3) \cdot (-0.002) = +0.0055 >> |-0.0005|$.

7.2 The damped mass-load

In this section, the bridge's motion under the action of a damped mass-load is studied. Given that the lateral motion is the same for both cases of loading, one may study the vertical-torsional motion and then compare the motion of the bridge under the action of a concentrated load and of a damped mass-load.

The plots of Fig. 16 show the influence of the speed υ on the vertical-torsional motion of the middle of the bridge for $R = 150$ m and $e_H = 3$ m.

From the above plots, one can see the strong influence of the speed on the dynamic lateral-torsional motion of the bridge.

The plots of Figs 17, 18, 19 show the motion of the middle of the bridge under the action of a concentrated load

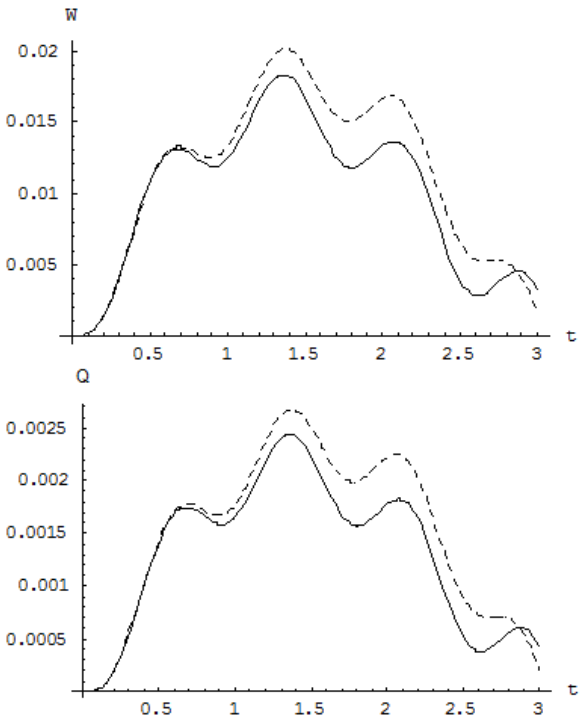

Figure 18: The influence of the load model for $R = 150$ m and $\upsilon = 20$ m/s and (- - -) Concentrated load $P = Mg$, (___) Damped mass-load M.

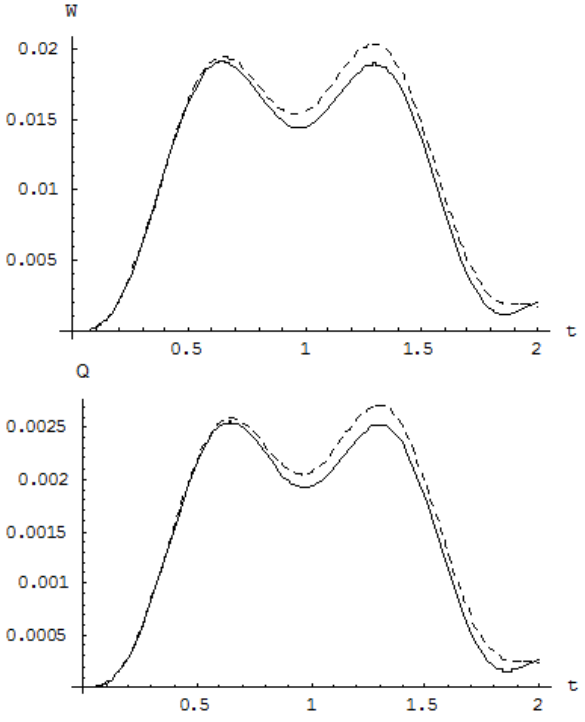

Figure 19: The influence of the load model for $R = 150$ m and $\upsilon = 30$ m/s and (- - -) Concentrated load $P = Mg$, (___) Damped mass-load M.

$P = M * g$ and a damped mass-load M for $R = 150$ m and different speeds.

From the above plots, is clear that the model of the damped mass-load gives more favorable results compared with the ones of the model of a simple concentrated load.

These differences, for small values of radii of curvature are approximately ~25%, decreasing for bigger radii to ~5%.

7.3 The moving vehicle

In this section, the dynamic behavior of the bridge shown in Fig. 5a, under the action of a vehicle like the one of Fig. 5b, is studied.

7.3.1 The lateral motion

- The influence of the load model

The plots of Fig. 20 show the lateral motion of the middle of the bridge (at $x = L/2$), for $\upsilon = 30$ m/s, $e_H = 3.00$ m, $e_V = 1.20$ m and various radii of curvature.

From the above plots, it is clear that the radius of curvature has small effect on the lateral vibrations of the bridge. This effect varies from 6 to 10%.

- The influence of length $2d$

The plots of Fig. 21 show the lateral motion of the middle of the bridge (at $x = L/2$), for $R = 50$ m, $\upsilon = 30$ m/s, $e_H = 3.00$ m, $e_V = 1.20$ m and various values of the vehicle length 2d.

The plots of Fig. 22 show the lateral motion of the middle of the bridge (at $x = L/2$), for $R = 100$ m, $\upsilon = 30$ m/s, $e_H = 3.00$ m, $e_V = 1.20$ m and various values of the vehicle length $2d$.

The plots of Fig. 23 show the lateral motion of the middle of the bridge ($x = L/2$), for $R = 150$ m, $\upsilon = 30$ m/s, $e_H = 3.00$ m, $e_V = 1.20$ m and various values of the vehicle length $2d$.

From the above plots, one can see that the vehicle's long has small effect on the lateral vibrations of the bridge. This effect varies from 4 to 8%.

7.3.2 The vertical-torsional motion

- The model influence

The plots of Fig. 24 show the vertical-torsional motion of the middle of the bridge (at $x = L/2$), for $R = 50$ m,

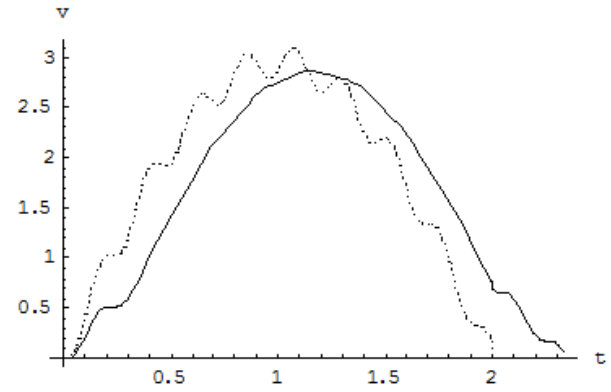

(a) $R = 50$ m

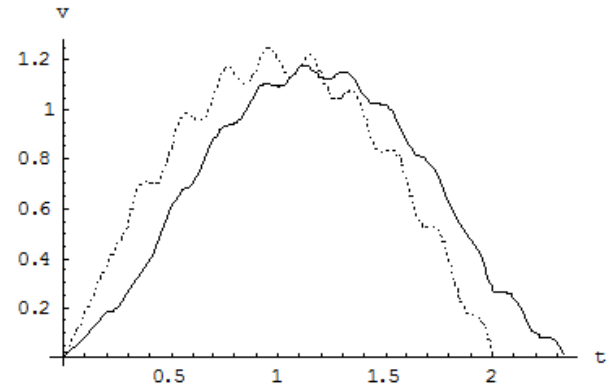

(b) $R = 100$ m

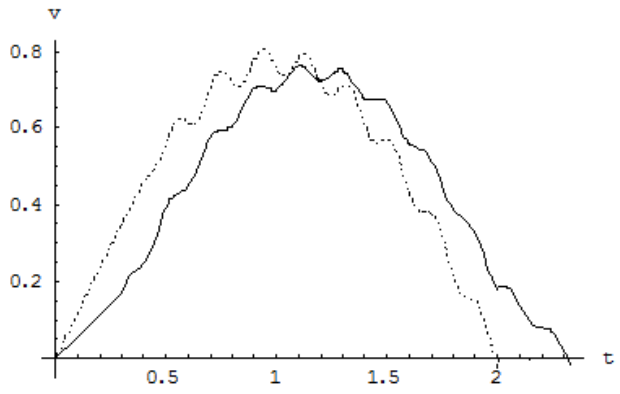

(c) $R = 150$ m

Figure 20: The influence of the load model for $\upsilon = 30$ m/s, $e_H = 3.00$ m, $e_V = 1.20$ m, for a vehicle with $2d = 10$ m (___), one concentrated load (- - -).

$\upsilon = 30$ m/s, $e_H = 3.00$ m, $e_V = 1.20$ m and three models of loading: one model of a real vehicle with dimensions $2d \cdot 2b$, a second model consisting of two concentrated loads and a third model consisting of one concentrated load. It is observed that for this value of R the differences are significant.

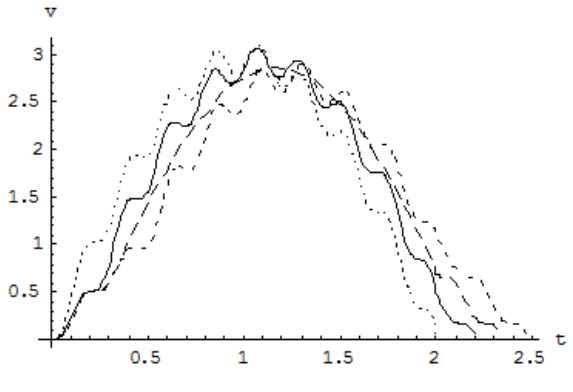

Figure 21: The influence of the vehicle length for $R = 50$ m, $\upsilon = 30$ m/s, $e_H = 3.00$ m, $e_V = 1.20$ m and $d = 3$ m (__), $d = 5$ m (_ _), $d = 7$ m (- - -) and $d = 0$ m (. . . .).

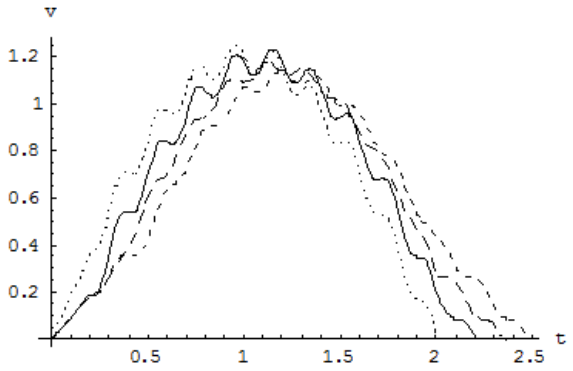

Figure 22: The influence of the vehicle length for $R = 100$ m, $\upsilon = 30$ m/s, $e_H = 3.00$ m, $e_V = 1.20$ m and $d = 3$ m (__), $d = 5$ m (_ _), $d = 7$ m (- - -) and $d = 0$ m (. . . .).

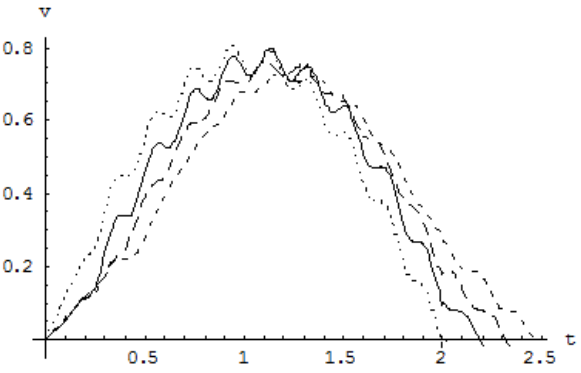

Figure 23: The influence of the vehicle length for $R = 150$ m, $\upsilon = 30$ m/s, $e_H = 3.00$ m, $e_V = 1.20$ m and $d = 3$ m (__), $d = 5$ m (_ _), $d = 7$ m (- - -) and $d = 0$ m (. . . .).

The plots of Fig. 25 show the vertical-torsional motion of the middle of the bridge (at $x = L/2$), for $R = 100$ m, $\upsilon = 30$ m/s, $e_H = 3.00$ m, $e_V = 1.20$ m and the same as above three models of loading.

The plots of Fig. 26 show the vertical-torsional motion of the middle of the bridge (at $x = L/2$), for $R = 100$ m,

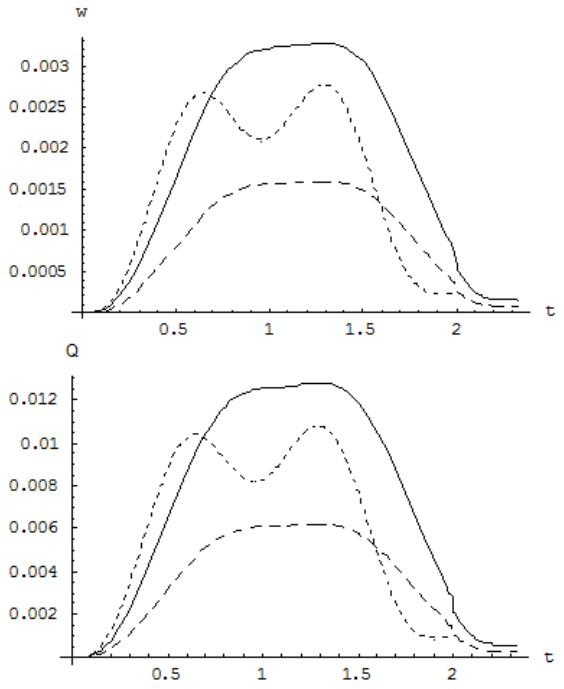

Figure 24: The vertical-torsional motion of the middle of the bridge (at $x = L/2$), for $R = 50$ m, $v = 30$ m/s, $e_H = 3.00$ m, $e_V = 1.20$ m and three models of loading (__) the real vehicle, (- - -) sequence of two loads, (. . . .) one concentrated load.

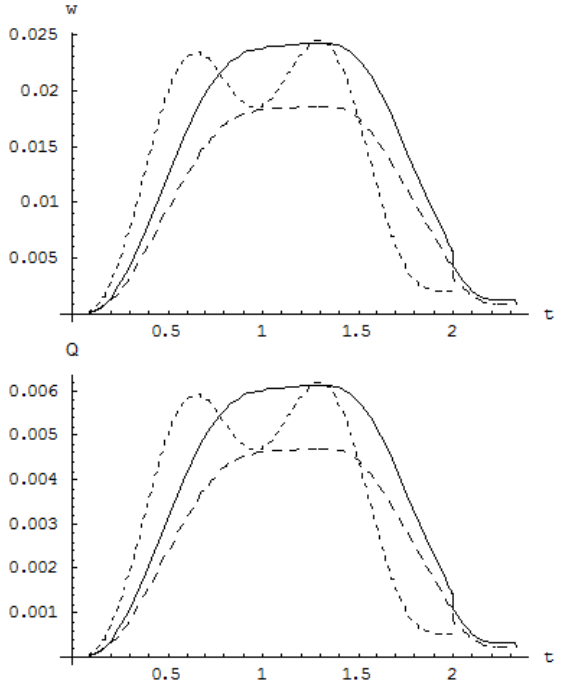

Figure 25: The vertical-torsional motion of the middle of the bridge (at $x = L/2$), for $R = 100$ m, $v = 30$ m/s, $e_H = 3.00$ m, $e_V = 1.20$ m and three models of loading (__) the real vehicle, (- - -) consequence of two loads, (. . . .) one concentrated load.

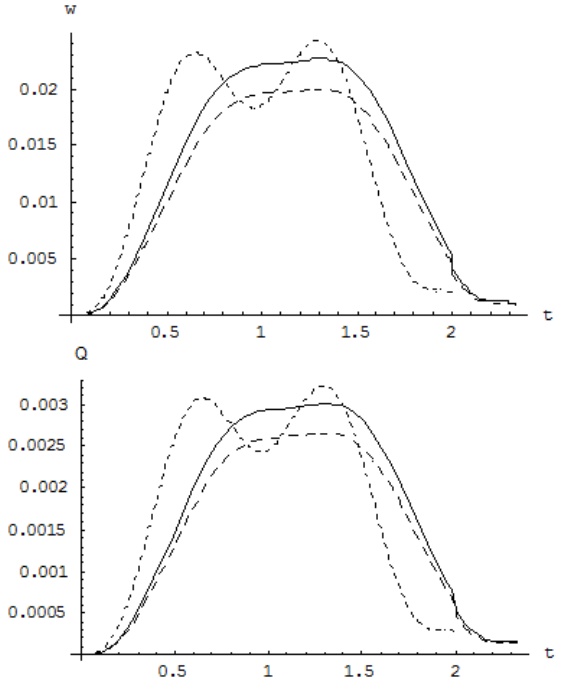

Figure 26: The vertical-torsional motion of the middle of the bridge (at $x = L/2$), for $R = 150$ m, $v = 30$ m/s, $e_H = 3.00$ m, $e_V = 1.20$ m and three models of loading (__) the real vehicle, (- - -) consequence of two loads, (. . . .) one concentrated load.

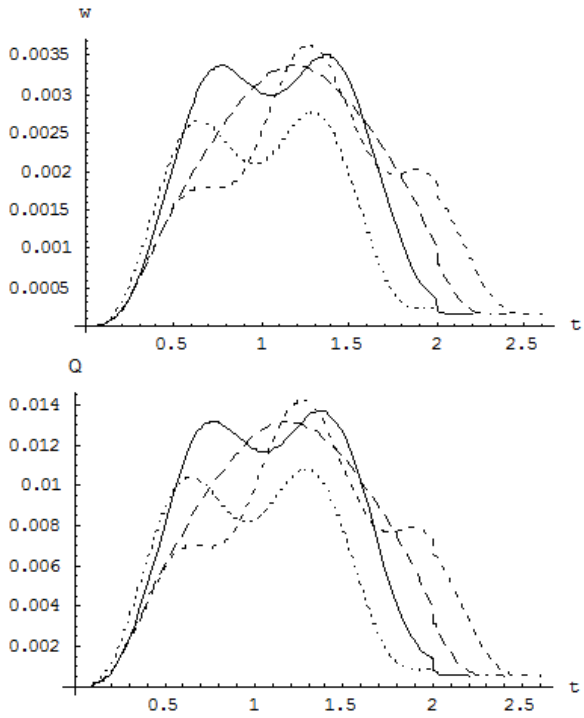

Figure 27: The influence of the vehicle length for $R = 50$ m, $v = 30$ m/s, $e_H = 3.00$ m, $e_V = 1.20$ m and $d = 3$ m (__), $d = 5$ m (_ _), $d = 7$ m (- - -) and $d = 0$ m (. . . .).

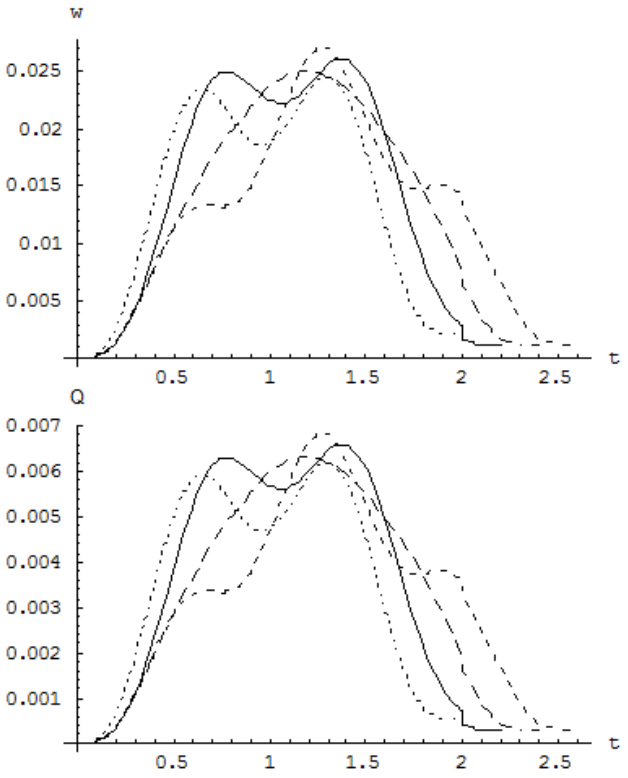

Figure 28: The influence of the vehicle length for $R = 100$ m, $\upsilon = 30$ m/s, $e_H = 3.00$ m, $e_V = 1.20$ m and $d = 3$ m (__), $d = 5$ m (_ _), $d = 7$ m (- - -) and $d = 0$ m (. . . .).

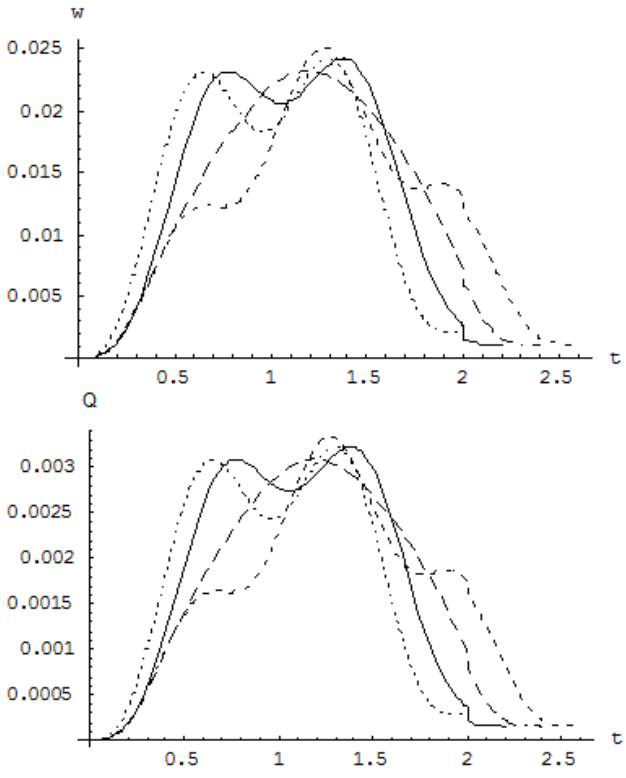

Figure 29: The influence of the vehicle length for $R = 150$ m, $\upsilon = 30$ m/s, $e_H = 3.00$ m, $e_V = 1.20$ m and $d = 3$ m (__), $d = 5$ m (_ _), $d = 7$ m (- - -) and $d = 0$ m (. . . .).

$\upsilon = 30$ m/s, $e_H = 3.00$ m, $e_V = 1.20$ m and the above three models of loading.

From Fig. 24, one can see that for small radii of curvature the choice of the right model significantly affects the dynamic response. It is also shown that the model with two concentrated loads leads to inaccurate results. This error amounts up to about 100%.

From the plots of Figs 25 and 26, it is shown that the above model of two loads produces the most inaccurate results with error from 15 to 25%.

- The influence of length $2d$

The plots of Fig. 27 show the lateral motion of the middle of the bridge (at $x = L/2$), for $R = 50$ m, $\upsilon = 30$ m/s, $e_H = 3.00$ m, $e_V = 1.20$ m and various values of the vehicle length $2d$.

The plots of Fig. 28 show the lateral motion of the middle of the bridge (at $x = L/2$), for $R = 100$ m, $\upsilon = 30$ m/s, $e_H = 3.00$ m, $e_V = 1.20$ m and various values of the vehicle length $2d$.

The plots of Fig. 29 show the lateral motion of the middle of the bridge (at $x = L/2$), for $R = 150$ m, $\upsilon = 30$ m/s, $e_H = 3.00$ m, $e_V = 1.20$ m and various values of the vehicle length $2d$.

From the above plots, on can see that for small radii of curvature ($R = 50$ m), the single concentrated load is the most inaccurate model (error ~20%). The rest three models give somewhat similar results.

For bigger radii of curvature ($R = 100$ m or 150 m), all models give similar results regarding the maximum deformations. The differences amount to about 3 to 6%. Note that each model gives a different view of the deformations of the bridge. For example, the models with $d = 3$ and $d = 5$ m give one maximum while the ones with $d = 0$ and $d = 7$ m give two maxima.

7.4 The damped vehicle

In this section, the dynamic behavior of the bridge shown in Fig. 5a, under the action of a vehicle like the one of Fig. 5c, is studied.

Given that the lateral motion is the same for both cases of loading (vehicle and damped vehicle), we will study the vertical-torsional motion and compare the motion of the bridge under the action of a simple vehicle and a damped vehicle.

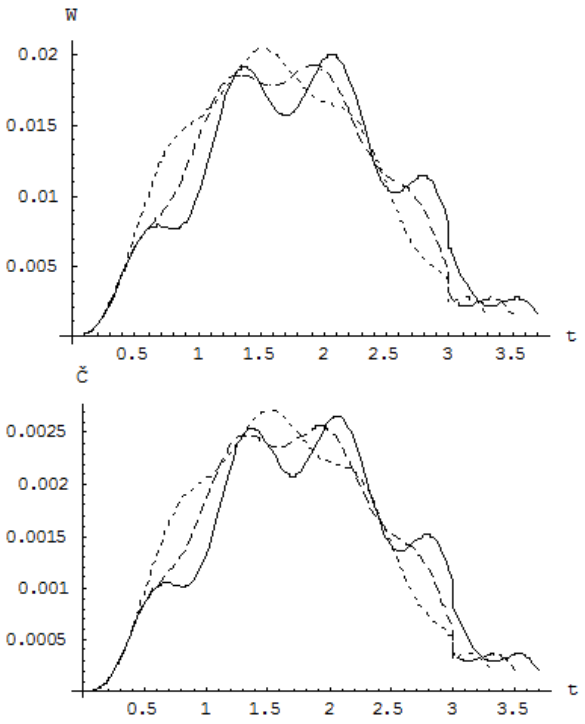

Figure 30: The influence of the vehicle length for $R = 150$ m, $\upsilon = 30$ m/s, $e_H = 3.00$ m, $e_V = 1.20$ m and $d = 7$ m (__), $d = 5$ m (_ _), and $d = 3$ m (- - -).

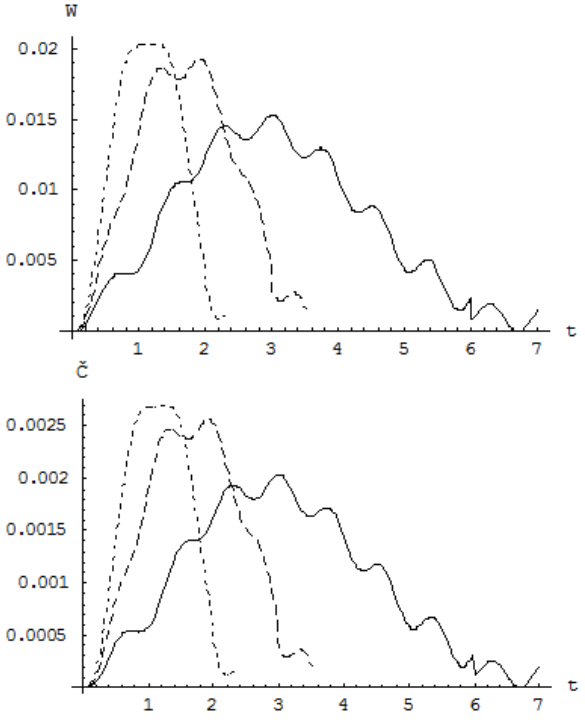

Figure 31: Influence of the speed υ for $R = 150$ m, $d = 5$ m, $e_H = 3.00$ m, $e_V = 1.20$ m and υ=10m/s (__), $\upsilon = 20$ m/s (_ _), and $\upsilon = 30$ m/s (- - -).

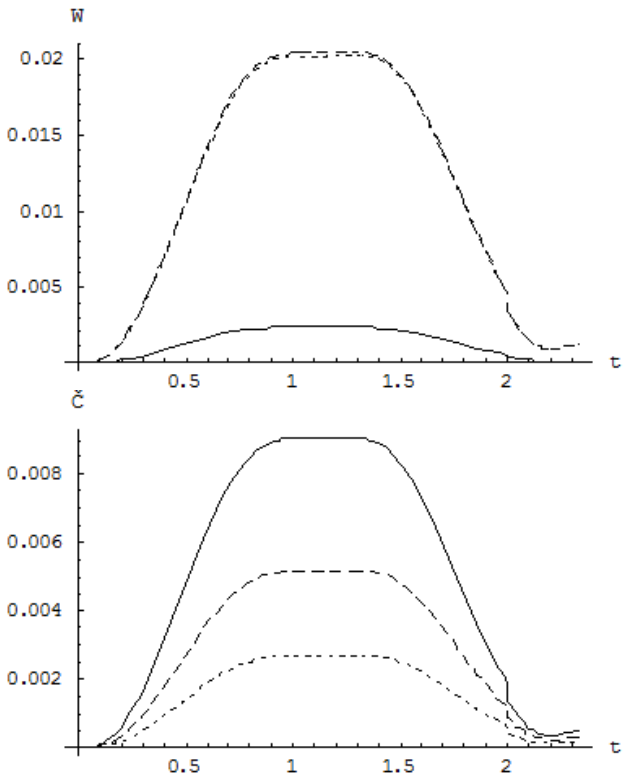

Figure 32: Influence of the radius of curvature R for $d = 5$ m, $e_H = 3.00$ m, $e_V = 1.20$ m $\upsilon = 30$ m/s and $R = 50$ m (__), $R = 100$ m (_ _), and $R = 150$ m (- - -).

The plots of Fig. 30 show the vertical-torsional motion of the middle of the bridge (at $x = L/2$), for $R = 150$ m, $\upsilon = 30$ m/s, $e_H = 3.00$ m, $e_V = 1.20$ m and various values of the damped vehicle length $2d$.

From the above plots, it is ascertained that the wheel-base $2d$ strongly affects the dynamic behavior of the bridge, similarly as in the plots of Fig. 27.

The plots of Fig. 31 show the vertical-torsional motion of the middle of the bridge (at $x = L/2$), for $R = 150$ m, $d = 5$ m, $e_H = 3.00$ m, $e_V = 1.20$ m, and various speeds υ.

From the plots of Fig. 31, one can see that the speed υ strongly affects the dynamic behavior of the bridge.

The plots of Fig. 32 show the vertical-torsional motion of the middle of the bridge (at $x = L/2$), for $d = 5$ m, $e_H = 3.00$ m, $e_V = 1.20$ m, $\upsilon = 30$ m/s and various radii of curvature R.

From the plots of Fig. 32, it can be deduced that for small radii of curvature the vertical motion is very small while the torsional one becomes maximum.

In contrast, quite the opposite is happening for big values of curvature radii.

The plots of Fig. 33, 34 and 35 show the vertical-torsional motion of the middle of the bridge (at $x = L/2$), for $R = 150$ m, $d = 5$ m, $e_H = 3.00$ m, $e_V = 1.20$ m and

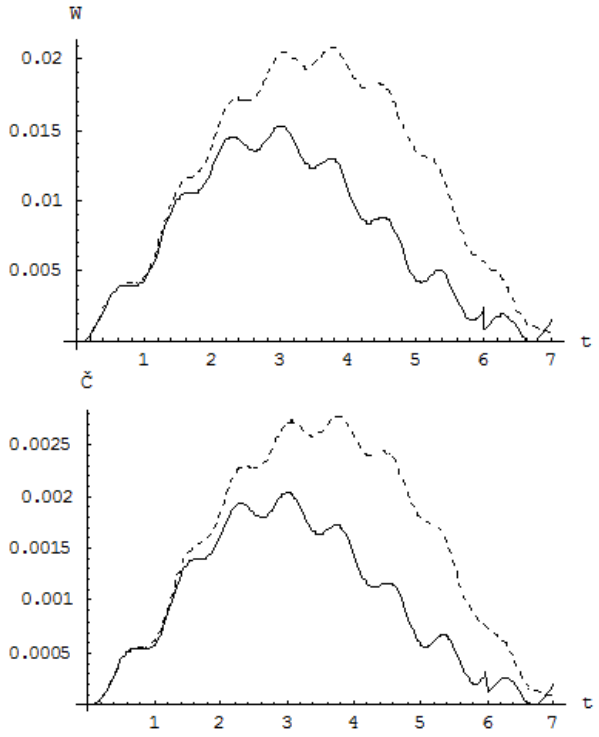

Figure 33: The vertical-torsional motion of the middle of the bridge for υ = 10 m/s and for damped vehicle (__) , simple vehicle (- - -).

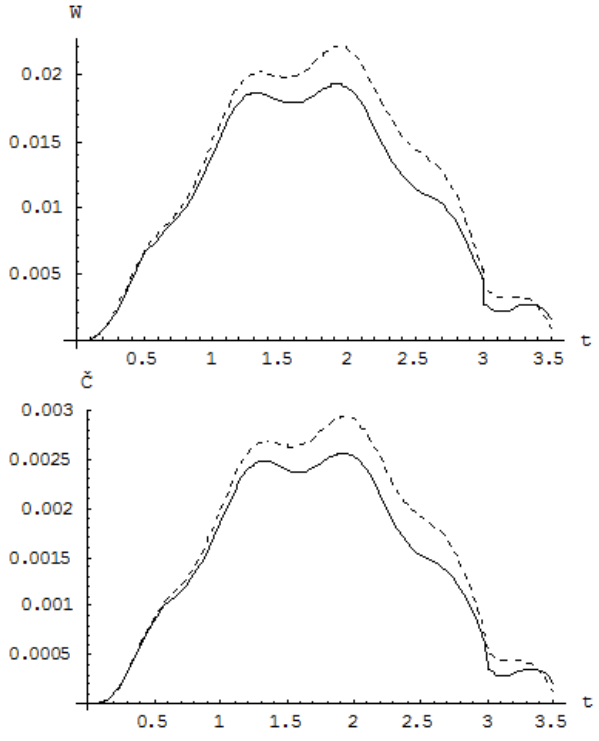

Figure 34: The vertical-torsional motion of the middle of the bridge for υ = 20 m/s and for damped vehicle (__) , simple vehicle (- - -).

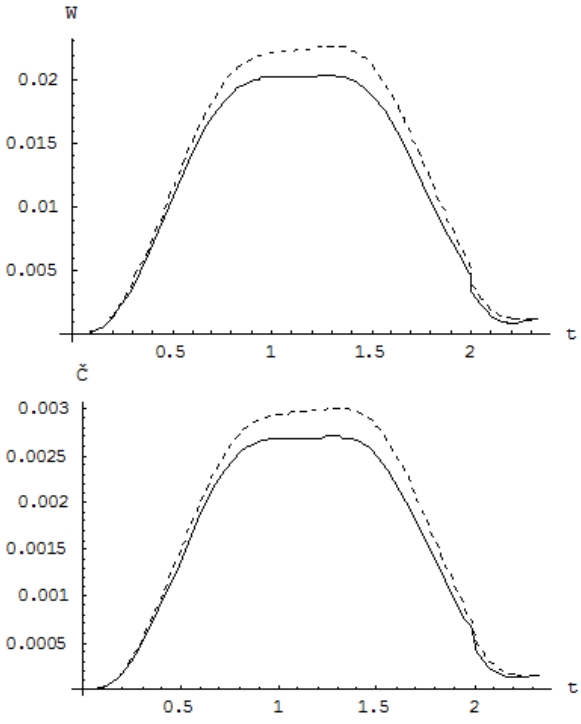

Figure 35: The vertical-torsional motion of the middle of the bridge for υ = 30 m/s and for damped vehicle (__) , simple vehicle (- - -).

different values of speed υ under the action of a simple vehicle and of a damped vehicle.

From the above plots, one can see that the damped mass-load model produces more favorable results compared to the ones of the model with a simple concentrated load.

These differences, for small values of radii of curvature are approximately ~35% and decrease for bigger radii to ~12%.

Finally, the plots of Figs 36, 37 and 38 show the vertical-torsional motion of the middle of the bridge (at $x = L/2$), for R = 50 m, R = 100 m, R = 150 m and d = 5 m, e_H = 3.00 m, e_V = 1.20 m, υ = 30 m/sunder the action of the four loading models.

The above plots show that the exact model of the damped vehicle gives for:

- small radii of curvature:
  - ~40% smaller deflections compared with the simple vehicle
  - ~20% smaller deflections compared with the simple load
  - ~10% smaller deflections compared with the damped load
- medium radii of curvature:

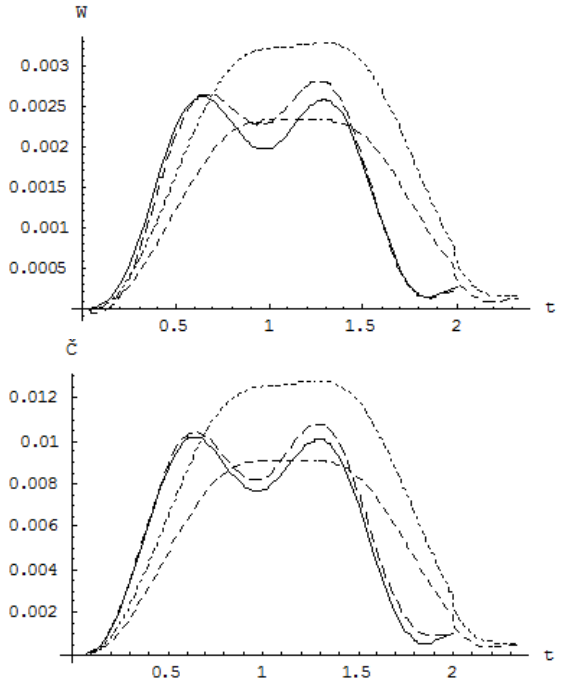

Figure 36: The vertical-torsional motion of the middle of the bridge, for $R = 50$ m, $d = 5$ m, $e_H = 3.00$ m, $e_V = 1.20$ m, $\upsilon = 30$ m/s, under the action of a Damped load (__), Simple load (_ _), Damped vehicle (- - -), Simple vehicle (. . . .).

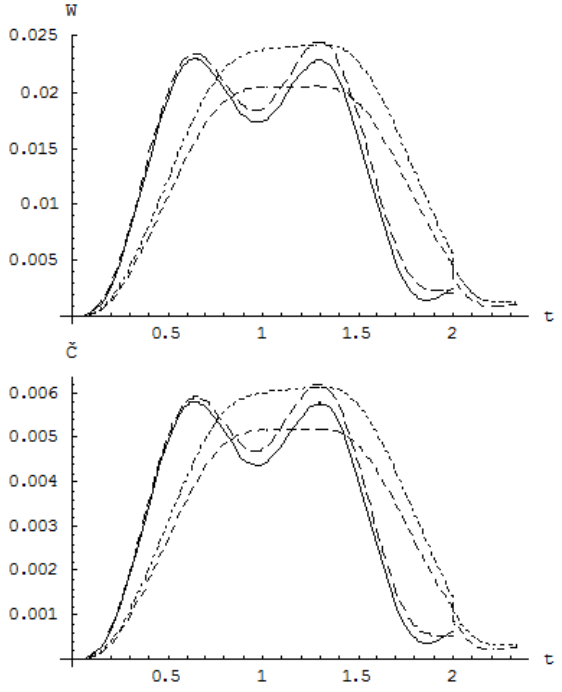

Figure 37: The vertical-torsional motion of the middle of the bridge, for $R = 100$ m, $d = 5$ m, $e_H = 3.00$ m, $e_V = 1.20$ m, $\upsilon = 30$ m/s, under the action of a Damped load (__), Simple load (_ _), Damped vehicle (- - -), Simple vehicle (. . . .).

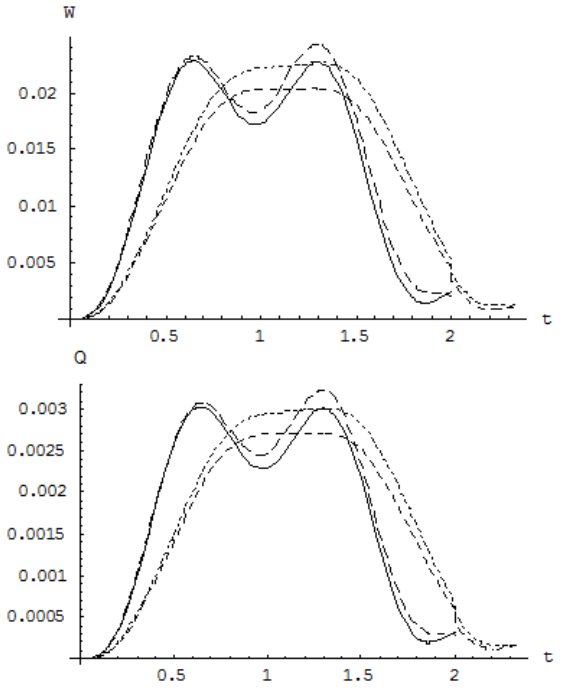

Figure 38: The vertical-torsional motion of the middle of the bridge, for $R = 150$ m, $d = 5$ m, $e_H = 3.00$ m, $e_V = 1.20$ m, $\upsilon = 30$ m/s, under the action of a Damped load (__), Simple load (_ _), Damped vehicle (- - -), Simple vehicle (. . . .).

~18% smaller deflections compared with the simple vehicle
~15% smaller deflections compared with the simple load
~10% smaller deflections compared with the damped load

– bigger radii of curvature:

~10% smaller deflections compared with the simple vehicle
~20% smaller deflections compared with the simple load
~10% smaller deflections compared with the damped load

8 Conclusions

From the preceding analysis and the models chosen herein, one can draw the following conclusions:

- A simple mathematical model for studying curved-in-plane bridges is presented.
- Regarding the deck surface conditions, it is shown that for wet surfaces the value of a safe speed decreases significantly (24 to 27% for $R = 50$ m

to 150 m), while the use of track cant angle improves noticeable the value of the allowed safe speed (~16%).

- The radius of curvature strongly affects the lateral motion of the bridge.
- For the vertical-torsional motion and for small values of the radius of curvature, negative deflections of the bridge's axis are sometimes observed, while the deflections of the points where the load applies is positive with values much bigger than the ones corresponding to the bridge axis.
- The above mentioned deformations are affected by the eccentricity of the applied load, and this influence amounts from 3 to 15%.
- In bridges with small radii of curvature, one should use load models approaching, as possible, the actual vehicle. In this case, it is recommended to avoid using the model of one concentrated load, or the one of a simple vehicle without a damping system, because the dynamical response error is extremely high.
- Regarding the distance of vehicle axles, the use of real data is crucial not only for determining the exact value of the maximum deflection but also to achieve the correct view of the bridge deflections.
- For ratios L/2d >~ 7, the resulting maximum values of deformations are not severely affected by the use of a specific load model.
- In all cases, the use of the exact load model of the damped vehicle is recommended, since it clearly produces the most accurate results, mainly for small radii of curvature. For bigger radii, one can employ the damped concentrated load with an error from 9 to 11%.
- The use of the simple vehicle model is not recommended in the case of small radii of curvature, since the error may reach up to 40%.
- The above mentioned errors are all in favor of safety, since the dynamical deformations are all bigger than the ones obtained with simplified models.

References

[1] Frýba, Vibrations of solids and structures under moving loads, Nordhoff International Publication Co, Groningen, The Netherlands, 1972

[2] G.G. Stokes, Discussion of a differential equation relating to the breaking of railway bridges, Transactions of the Cambridge Philosophical Society (1849) 707–735

[3] H. Zimmermann, Die Schwingungen eines Trägers mit bewegter Last, Centralblatt der Bauverwaltung, 16 (1896) 249–251

[4] A.N. Krýlov, Über die erzwungenen Schwingungen von gleichförmigen elastigchen Stäben, Mathematical Annalen, 61 (1905) 211

[5] S.P. Timoshenko, On the forced vibration of bridges, Philosophical Magazine, Series 6, 43 (1922) 1018

[6] C.E. Inglis, A Mathematical Treatise on Vibration in Railway Bridges, The University Press, Cambridge, 1934

[7] A. Hillerborg, Dynamic influences of smoothly running loads of simply supported girders, Kungl. Tekhn. Högs kolan, Stockholm, 1951

[8] H. Steuding, Die Schwingungen von Trägern bei bewegten Lasten I, II", Ingenieur Archiv, 5(4) (1934) 275-305 and 6(4) (1935) 265–270

[9] H. Honda, Y. Kajikawa, T. Kobori, Spectra of road surface roughness on bridges, Journal of Structural Engineering ASCE, 108(9) (1982) 3231–3243

[10] T.D. Gillespi *et al.*, Effect of heavy vehicle characteristics on pavement response and performance, NCHRP, Rep. 353, (1993) Trans Res. Board (TRB), Washington D.C.

[11] M.F. Green, D. Cebon, D.J. Cole, Effects of Vehicle Suspension Design on Dynamics of highway Bridges, Journal of Structural Engineering, 121(2) (1995) 272–282

[12] H.P. Lee, Dynamic response of a Beam with a moving mass, Journal of Sound and Vibration, 191(2) (1996) 289–294

[13] G.T. Michaltsos, D. Sophianopoulos, A.N. Kounadis, The effect of a moving mass and other parameters on the dynamic response of a simply supported beam, Journal of Sound and Vibration, 191(3) (1996) 357–362

[14] X. Xu, W. Xu, J. Genin, A non linear moving mass problem, Journal of Sound and Vibration, 204(3) (1997) 495–504

[15] M.A. Foda, Z. Abduljabbar, A Dynamic Green Function Formulation for the response of a Beam structure to a moving Mass", Journal of Sound and Vibration, 210(3) (1998) 295–306

[16] G.T. Michaltsos, The influence of Centripetal and Coriolis forces on the dynamic response of light bridges under moving vehicles, Journal of Sound and Vibration, 247(2) (2001) 261–277

[17] G.T. Michaltsos, Dynamic behaviour of a single-span beam subjected to load moving with variable speeds, Journal of Sound and Vibration, 258(2) (2002) 359–372

[18] Am. Association of State Highway and Transport. Officials (AASHTO), Standard specifications for highway bridges, 12th edition, Washington D.C., 1977

[19] Ministry of Transport. and Communications, Ontario highway bridge design code, Downsview, Ontario, Canada, 1983.

[20] Council of Eur. Communities, Council Directive, 92/7/EEC amending Directive 85/3/EEC on the weights, dimensions and certain technical characteristics of certain road vehicles, Brussels, Belgium, 1992

[21] ISO/TC 108/WG9 Draft No 3c, Proposals for generalized road inputs to vehicles, Int. Organization for Standarization (ISO), Geneva, Switzerland, 1972

[22] R. Cantieri, Beitrag zur dynamik von Strassenbrucken unter der uberfahrt schwerer Fahrzeuge, Diss. ETH Nr 9505, Technische Hochschule, Zurich, 1991

[23] J. Mozer, C. Culver, Horizontally curved highway bridges –S tability of curved plate girders, Report no.P1, research project HPR-2(111), Carnegie Mellon University, Pittsburgh, 1970

[24] C. Culver, Design recommendations for curved highway bridges, Final report for research project 68-32, Pennsylvania Department of Transportation, Harrisburg, PA, 1972
[25] P.J. Brennan, Analysis and structural testing of a multiple configuration small scale horizontally curved highway bridge, Research project HPR-2(111), Syracuse University, Syracuse, NY, 1974
[26] C.H. Yoo, R.L. Carbine, Experimental investigation of horizontally curved steel wide flange beams analysis, In: Proceedings structural stability research council annual technical session: stability aspects of industrial buildings, (1985) 183–191
[27] A. Zureick, R. Naqib, J.M. Yadlosky, Curved steel bridge research project, interim report I: synthesis, HDR Engineering, Pittsburgh. Publication Number FHWA-RD-93-129, 1994
[28] CEN, Eurocode 8. Design of structures for earthquake resistance: Part 2. Bridges. CEN, Brussels, 2006
[29] Caltrans, Seismic design criteria 1.4, California Department of Transportation, Sacramento, CA, 2006
[30] M.N. Abdel-Salam, C.P. Heins, Seismic response of curved steel box girder bridges, J Struct Eng, 114(12) (1988) 2790–2800
[31] H. Wu, W.S. Najjar, Parametric seismic analysis of curved steel box-girder bridges with two continuous spans, Bridge Struct 3(3,4) (2007) 205–213
[32] D.G. Linzell, V.P. Nadakuditi, Parameters influencing seismic response of horizontally curved steel I-girder bridges, Steel Compos Struct, 11(1) (2011) 21–38
[33] G. Dimitrakopoulos, Q. Zeng, A three-dimensional dynamic analysis scheme for the interaction between trains and curved railway bridges, Computers and Structures, 149 (2015) 43–60
[34] N. Tondini, B. Stojadinovic, Probabilistic seismic demand model for curved reinforced concrete bridges, Bul Earthquake Eng, 10 (2012) 1455–1479
[35] T. Avraam, G.T. Michaltsos, The influence of curvature and other parameters on the dynamic behavior of curved bridges, Int. Journal of Bridge Engineering, 3(2) (2015) 49–76
[36] I. Raftoyiannis, G.T. Michaltsos, Curved-in-plane Cable-Stayed Bridges. A mathematical model, Int. Journal of Struct. Stability and Dynamics, 12(3) (2012) DOI: 10.1142/S0219455412500113
[37] A.N. Kounadis, An efficient and simple approximate technique for solving non-linear initial and boundary-value problems, Comp. Mechanics, 9 (1992) 221–231